Magnetic resonances in atomic hydrogen

Pro gradu -tutkielma
Turun yliopisto
Fysiikan laitos
Fysiikka
2005
Janne Ahokas
Tarkastajat:
Prof. Reino Laiho
Dos. Simo Jaakkola

TURUN YLIOPISTO
Fysiikan Laitos

AHOKAS, JANNE Magnetic resonances in atomic hydrogen

Pro Gradu -tutkielma, 47 s.
Fysiikka
Joulukuu 2005

Tutkielmassa perehdytään magneettisen resonanssin menetelmien elektronin spin-resonanssin (ESR) sekä ydinmagneettisen resonanssiin (NMR) mahdollisuuksiin atomisen vetykaasun tutkimuksessa. Aluksi tutustutaan metastabiiliin atomiseen vetyyn sekä magneettisen resonanssin menetelmiin. Seuraavaksi tarkastellaan vetyä eri ympäristöissä, joissa sitä tutkittiin kokeellisesti. Kokeellisen osion alussa on johdanto koelaitteistoon, jonka jälkeen esitellään tehdyt mittaukset. Työssä suoritettiin ensimmäiset ESR- ja NMR-mittaukset molekylaariseen vetyyn stabiloidussa atomisessa vetykaasussa (H_M).

Yksinkertaisimpana atomina vety on mielenkiintoinen tutkimuskohde niin teoreettisesti kuin kokeellisesti. Nestemäisen heliumin pinnalle adsorboituneet vetyatomit muodostavat ainutlaatuisen kaksiulotteisen (2D) systeemin. Atominen vety kiinteän molekylaarisen vedyn sisällä havaittiin hiljattain hyvin stabiiliksi, mikä mahdollistaa kyseisessä systeemissä tarpeeksi matalissa lämpötilossa suprajuoksevan (suprakiinteän) käytöksen etsimisen.

ESR:n tavanomainen sovellus on atomien tilatiheyksien määritys. Nestemäisen heliumin pinnalle adsorboituneen 2D vetykaasun kompressiokokeissa pystytään ESR:llä havaitsemaan suoraan vapaan kolmiulotteisen (bulk) vetykaasun sekä adsorboituneen 2D vetykaasun tiheys. Tässä työssä toteutetulla vedyn NMR-transition kalorimetrisella havaintomenetelmällä olisi suuremmalla herkkyydellä mahdollista havaita ESR:stä riippumattomasti 2D-vedyn viivan siirtymä bulk-viivasta.

Aikaisemmissa ESR-mittauksissa havaittiin, että hyperhieno vuorovaikutus on heikompi H_M:lle kuin vapaalle H:lle. Tarkempi mittaus hyperhienon vuorovaikutusvakion muutokselle suoritettiin tässä työssä NMR:llä. NMR-transitio havaittiin ESR:llä atomien tilatiheyksien muutoksesta. Määritetty hyperhienon vuorovaikutusvakion muutos on $\Delta a/h = -1.3 \pm 0.06\,\mathrm{MHz}$. H_M:n havaittu NMR-transitio on varsin kapea, mikä kertoo H_2:n säännöllisestä kiderakenteesta. Paremmalla signaali/kohina-suhteella voitaisiin elektroni-ydin kaksoisresonanssi (ENDOR) -menetelmää hyödyntäen määrittää H_M:n hyperhieno rakenne tarkemmin.

Asiasanat: atominen vety, elektronin spin-resonanssi, ydinmagneettinen resonanssi

Contents

Introduction

Atomic hydrogen is the lightest of the atoms and the most common element in the universe. Due to its low mass and weak interactions, H is predicted to stay gaseous when temperature approaches to the absolute zero [1]. H atom is simple so that its properties and interactions can be calculated from the first principles, which makes it an interesting subject of experimental and theoretical studies. A unique property of H is that it may form a weakly interacting two-dimensional (2D) gas on the liquid helium surface [2]. Long term goals in hydrogen research have been an observation of the Bose-Einstein condensation (BEC) in bulk gas and the so-called quasicondensate (QC) in the H gas adsorbed on the liquid helium surface. Signatures of the QC formation in 2D H gas were observed at the University of Turku in 1998 [3] and BEC in H gas was observed at the MIT in 1998 [4]. Since that there have been attempts to observe the QC directly in the 2D H gas by ESR and optical methods [5, 6].

Magnetic resonance methods electron-spin resonance (ESR) and nuclear-magnetic resonance (NMR) have proved to be useful tools in studies of atoms and molecules having non-zero electron and/or nuclear magnetic moments. Typically information is obtained of magnetic susceptibility, atomic structure of the sample and processes in it at atomic level. Hydrogen atom has both electron and nuclear magnetic moments non-zero, and magnetic resonance methods have been used in its research since the first stabilization [1]. Bulk (3D) [1] and 2D H gas [7] densities are directly measured by ESR. NMR has been used to detect spin exchange effects in bulk H gas [8] and to manipulate energy state populations [9, 10]. ESR spectra of H in solid matrices give useful information on the positions and interactions of the atoms with host molecules of the matrix.

Recently H gas in H_2 crystals (H_M) at temperatures around 100 mK was found to be very stable against recombination [11], unlike in other experiments made at temperatures above 1 K [12]. A H_M layer is created in bulk H gas experiments on

the sample cell walls, and it can be detected simultaneously with bulk H gas by ESR. At low enough temperatures this system may show supersolid behavior [11], which has been recently observed in ^{4}He and H_2 crystals at temperatures below 150 mK [13]. A possibility of detecting quantum degenerate phenomena in H_M is the main interest in the studies of this system, but in order to reach these effects, one has to study and understand basic properties of the H_M system at low temperatures. First measurements of the hyperfine interaction change of H atoms in H_2 from that of the free atoms and information on the H_2 crystal quality are presented in this work.

The main purpose of this thesis is to understand how can modern techniques of the magnetic resonance methods ESR, NMR and electron-nuclear double resonance (ENDOR) be applied to study the H gas. The thesis is organized as follows. First I present an introduction to the properties of the metastable atomic hydrogen gas and magnetic resonance methods. Next, I consider H in different systems (environments), where we can study it by magnetic resonance methods. Then I present our experimental setup and experiments. Last section concerns the results of our ESR and NMR experiments on bulk and 2D H gas, and on H atoms inside solid H_2 crystals.

Some of the results included in this thesis are published as:
J. Järvinen, J. Ahokas, S. Jaakkola, and S. Vasilyev, Three-body recombination in two-dimensional atomic hydrogen gas, Phys. Rev. A 72, 052713 (2005).

1 Atomic hydrogen

1.1 Hydrogen atom in magnetic field

We consider the ground electron state of hydrogen atom (H). Its interaction with magnetic field is described by the Hamiltonian

$$\hat{\mathrm{H}} = g_e \mu_B \hat{\mathbf{S}} \cdot \mathbf{B} - g_n \mu_n \hat{\mathbf{I}} \cdot \mathbf{B} + a \hat{\mathbf{I}} \cdot \hat{\mathbf{S}}. \tag{1}$$

The first and second terms are the Zeeman interaction terms of electron and nucleus. The third term is the hyperfine interaction of electron and nucleus. g_e and μ_B are the g-factor and Bohr magneton for electron, g_n and μ_n are respectively the quantities for nucleus and a is the hyperfine coupling constant. The numerical values are presented in table 1.

Due to spins of electron and nucleus, the ground state is degenerate. Coupling between the electron and nuclear spins, or in classical terms the magnetic interaction of electron and nuclear magnetic moments, leads to the hyperfine structure of the ground state of hydrogen atom.

The interaction between electron and nucleus in H is called the isotropic contact

Table 1: Fundamental constants.

g_e	Electron g-factor	2.002 319 304 3718	[14]
μ_B	Bohr magneton	$9.274\,009\,49 \times 10^{-24}$ J/T	[14]
$g_e\mu_B$		$1.856\,952\,28 \times 10^{-23}$ J/T	
g_n	Proton g-factor	5.585 694 701	[14]
μ_n	Nuclear magneton	$5.050\,783\,43 \times 10^{-27}$ J/T	[14]
$g_n\mu_n$		$2.281\,213\,42 \times 10^{-26}$ J/T	
$g_n\mu_n/g_e\mu_B$		$1.519\,270\,38 \times 10^{-3}$	
a/h	Hyperfine interaction constant	1420.405 751 773 MHz	[1]
h	Plack constant	$6.626\,0693 \times 10^{-34}$ Js	[14]
k_B	Boltzmann constant	$1.380\,6505 \times 10^{-23}$ JK^{-1}	[14]

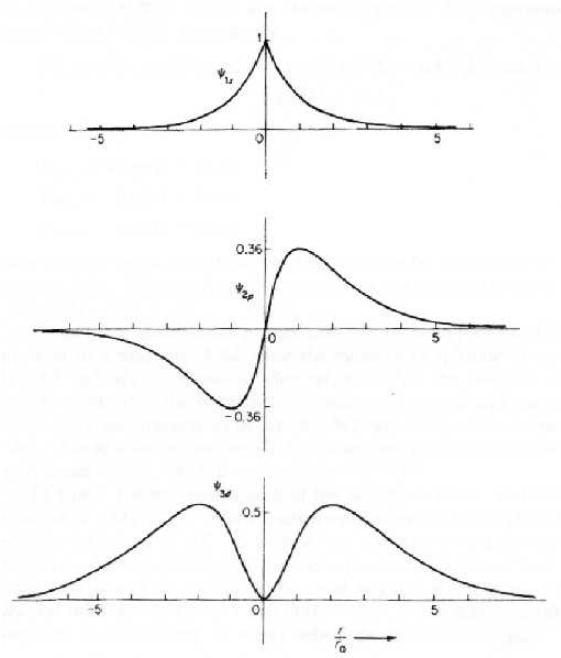

Figure 1: Electronic wave functions for states 1s, 2p and 3d [15].

interaction. The strength of the interaction has been calculated by Fermi [16]:

$$a = \frac{8\pi}{3} g_e \mu_B g_n \mu_n \left|\psi(0)\right|^2, \tag{2}$$

where $|\psi(0)|^2$ is the probability for electron to be at nucleus. Hyperfine interaction of electron and nucleus exist only when electron has nonzero probability to be at nucleus. In the case of H, this is true only when electron is in s-orbital. For other orbitals electron wave function is zero at the nucleus. Radial electron wave functions of 1s, 2p and 3d orbitals are presented in figure 1.

The hyperfine interaction splits the ground state of H to two states in zero magnetic field and to four states when an external field is applied. The hyperfine energy is $\sim 10^{-5}$ eV, much smaller than the energy of the excited electronic states (>10 eV).

In zero and low field the hyperfine coupling mixes the spin states and the total spin $\hat{\mathbf{F}} = \hat{\mathbf{I}} + \hat{\mathbf{S}}$ has to be used as quantum number describing the system. The state functions are of the form $|F, m_F>$, where $F = 0, 1$ is the magnitude and

$m_F = -F...F$ is the projection of $\hat{\mathbf{F}}$ along the quantization axis. In the high-field limit when $\frac{\mu^+ B}{a} \gg 1$, projections of the electron and nuclear spins $m_S, m_I = \pm\frac{1}{2}$ are also good quantum numbers. The state functions are now marked with $|m_S, m_I>$, where the spin quantum numbers are marked with $\uparrow$ corresponding to $\frac{1}{2}$ and $\downarrow$ corresponding to $-\frac{1}{2}$. The eigenstates of the Hamiltonian (1) are then

$$\begin{aligned} |a> &= \sin\theta|\uparrow\downarrow> - \cos\theta|\downarrow\uparrow> \\ |b> &= |\downarrow\downarrow> \\ |c> &= \cos\theta|\uparrow\downarrow> + \sin\theta|\downarrow\uparrow> \\ |d> &= |\uparrow\uparrow> . \end{aligned}$$

The wave function mixing parameter θ is defined by

$$\tan 2\theta = \frac{a}{\mu^+ B}. \tag{3}$$

In high field limit $\sin\theta$ can be approximated by

$$\varepsilon = \sin\theta \approx \frac{a}{4\mu_B B} \tag{4}$$

and similarly $\cos\theta \approx 1$.

The energies of the different states can be evaluated by calculating the eigenvalues of the energy matrix. This leads to a 4x4 matrix where elements can be calculated from

$$< m_S, m_I|\hat{\mathbf{H}}|m'_S, m'_I > .$$

The diagonal matrix elements are the eigenvalues of the states.

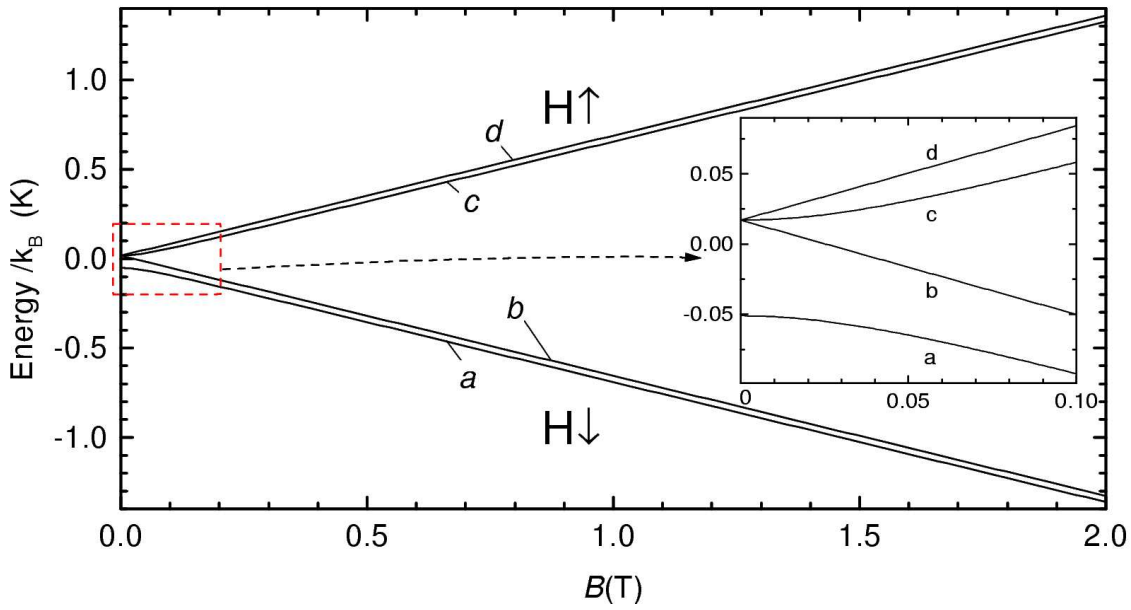

Figure 2: Hyperfine level diagram of atomic hydrogen in magnetic field [6].

Starting from the lowest the energies are

$$E_a = -\frac{1}{4}a - \frac{1}{2}a\sqrt{1+\left(\frac{\mu^+ B}{a}\right)^2} \tag{5}$$

$$\approx -\frac{1}{4}a - \frac{1}{2}\mu^+ B - \frac{a^2}{4\mu^+ B} \tag{6}$$

$$E_b = \frac{1}{4}a - \frac{1}{2}\mu^- B \tag{7}$$

$$E_c = -\frac{1}{4}a + \frac{1}{2}a\sqrt{1+\left(\frac{\mu^+ B}{a}\right)^2} \tag{8}$$

$$\approx -\frac{1}{4}a + \frac{1}{2}\mu^+ B + \frac{a^2}{4\mu^+ B} \tag{9}$$

$$E_d = \frac{1}{4}a + \frac{1}{2}\mu^- B, \tag{10}$$

where $\mu^\pm = g_e\mu_B \pm g_n\mu_n$. The energy levels in magnetic field are shown in figure 2. The electron spin-down states a and b are marked with H$\downarrow$ and the spin-up states c and d with H$\uparrow$. H$\downarrow$ atoms are pulled to a higher field and are therefore called high-field seekers, while H$\uparrow$ atoms are pushed away from the high field and are called low-field seekers.

1.2 Stabilization of atomic hydrogen gas

Being the lightest of alkalis, H is chemically very reactive substance and on earth hydrogen exists mainly in molecules. Two hydrogen atoms form a molecule with a binding energy of 52000 K, the largest known chemical reaction energy per mass unit. Atomic hydrogen was first stabilized in 1979 by Silvera and Walraven [17].

In the ground electronic state H atoms can interact via a singlet potential ($^1\Sigma_g^+$) or a triplet potential ($^3\Sigma_u^+$) (figure 3). Atoms with opposite electron spins interact via the singlet potential, which supports about 100 bound molecular states, having different rotational and vibrational energies. Due to the Pauli principle two electrons in same spin state state cannot form a molecule. Therefore H atoms with parallel electron spins interact via the repulsive triplet potential.

The key to stabilize H at high densities is to polarize the spins of electrons and thereby to remove the possibility for the atoms to form molecules. Electron-spin polarization can be achieved by applying a magnetic field to atoms at low temperatures. In a magnetic field B (figure 2) and at a temperature T the thermal population ratio of spin-up state (H$\uparrow$) to spin-down state (H$\downarrow$) is $\exp[-2\mu_B B/(k_B T)]$. For the field of 5 T and the temperature of 300 mK the ratio is $\sim 10^{-10}$. In practice, at $T < 1\,\mathrm{K}$ and $B \geq 5\,\mathbf{T}$ is enough to polarize and stabilize the sample.

A local maximum of magnetic field cannot be created in a free space. Therefore H$\downarrow$ sample has to be confined with walls. A local minimum can be created by a system of coils, which forms a magnetic trap for low-field seekers. Therefore, wall-free confinement of H$\uparrow$ atoms is possible. A disadvantage is that because atoms are not in the lowest energy state, they can relax in collisions to the electron spin-down state and be pushed away from the trap or recombine.

A vital thing to stabilize H in high fields is the surface with which atoms are in contact. Nearly all materials have so strong interaction with hydrogen atoms, that all atoms will adsorb on the surface and rapidly recombine. The only exception to this is liquid helium (liquid ^{4}He, LHe).

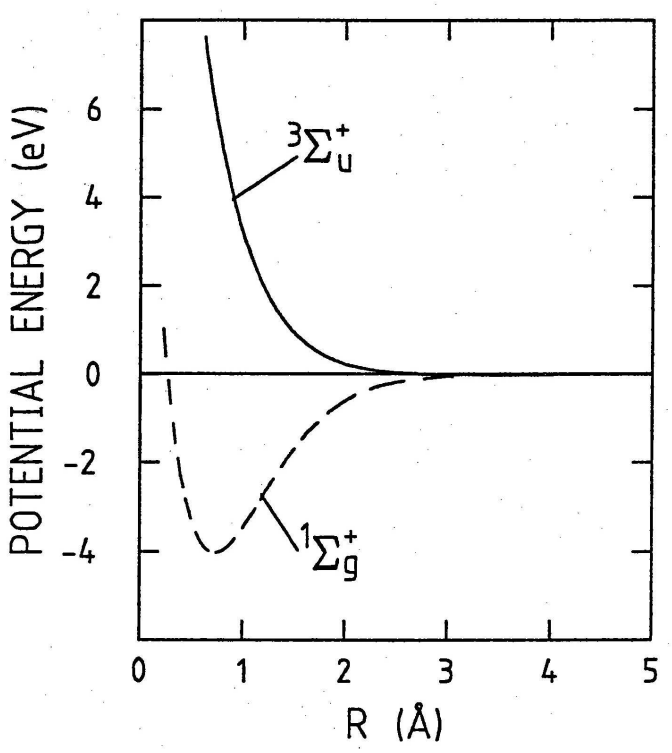

Figure 3: Singlet $^1\Sigma_g^+$ and triplet $^3\Sigma_u^+$ potentials [1].

1.3 Atomic hydrogen on the surface of liquid helium

Being the lightest of cryogenic liquids, ^{4}He (and it's lighter isotope ^{3}He) has the weakest interaction with H. Interaction potential between H and LHe supports only one bound state with the binding (adsorption) energy of $E_a/k_B = 1.14\,\mathrm{K}$ [10] (figure 4). Due to the short-range repulsive potential H atoms cannot dissolve into LHe. The potential that the H atoms feel is uniform in the plane and they can freely move as a 2D gas. There is a dynamic equilibrium between the atoms on the surface and the bulk gas above it driven by a rapid exchange of atoms between these two systems [2].

In a thermal equilibrium the density σ of 2D H gas adsorbed on LHe is given by the adsorption isotherm

$$\sigma = n\Lambda \exp \frac{E_a}{k_B T}, \tag{11}$$

where n is the bulk gas density and $\Lambda \approx 17.4 \times T^{-1/2}\,\mathrm{K}^{1/2}\mathrm{\AA}$ is the thermal de Broglie wavelength [2]. Even with the adsorption energy as low as 1.14 K, the density of

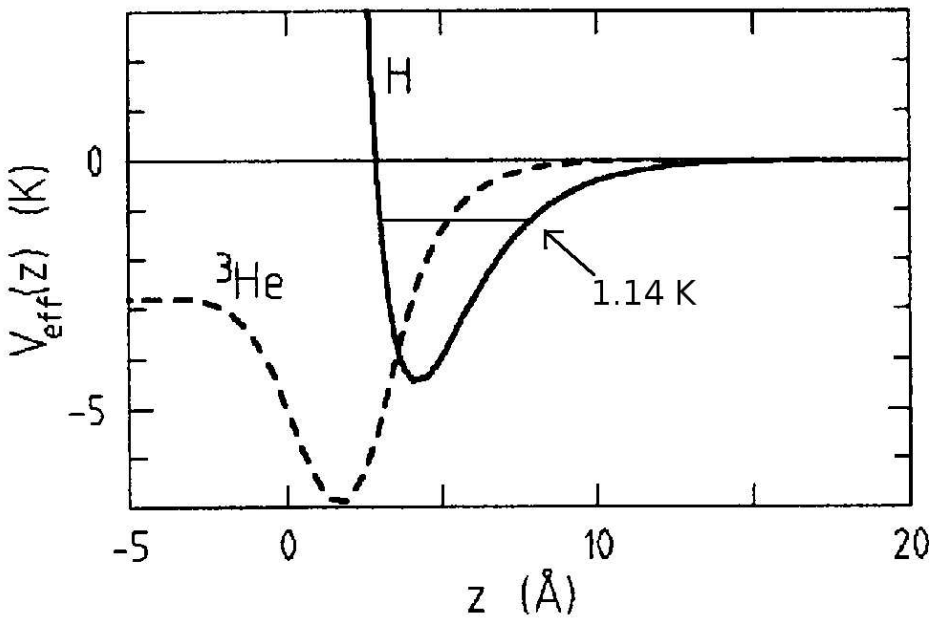

Figure 4: Interaction potential of H atom and ^{3}He atoms with LHe surface. ^{3}He can dissolve in ^{4}He but H cannot [2].

adsorbed atoms can become rather large, at $T \sim 100\,\mathrm{mK}$ and $n \sim 10^{13}\,\mathrm{cm}^{-3}$ the surface density is $\sigma \geq 10^{12}\,\mathrm{cm}^{-2}$.

1.4 Recombination of spin-polarized atomic hydrogen gas

Polarization of the electron spins of H atoms strongly decreases the recombination probability but not to zero, which makes the H$\downarrow$ gas metastable. There are several recombination mechanisms which occur in the bulk and on the surface. A third body is necessary to satisfy the momentum and energy conservation laws in a recombination event. At low bulk gas densities, $n \leq 10^{15}\,\mathrm{cm}^{-3}$ and temperatures of 100–200 mK, there is practically no ^{4}He vapor and three-body collisions of H atoms can be neglected. Therefore the surface of helium plays the role of the third body, and recombination takes place on it. If there are H$\uparrow$ atoms in the H$\downarrow$ sample, they will recombine rapidly on the surface in two-body collisions.

In an electron spin-polarized sample there is a similar, but slower recombination channel. If the sample contains mixed state a atoms, there is a probability that an a-state atom in a collision event is in the electron spin-up state. This allows

recombination in $a-a$ and $a-b$ collisions. The probability of finding an a-atom in the electron spin-up state in a field of 5 T is given by $\varepsilon^2 = [a/(4\mu_B B)]^2 \approx 3 \cdot 10^{-5}$. Despite of a such small probability this recombination channel is the fastest even at high fields. The preferential recombination of a-state leads to a doubly polarized sample H$\downarrow\downarrow$, containing only pure b-state [1].

A doubly polarized sample may decay via relaxation from b to a and three-body dipolar recombination $b-b-b \rightarrow H_2$. The relaxation occurs on the walls of sample cell. It is caused by an interaction of magnetic moments of H atoms with magnetic impurities embedded into the cell walls, or with a self-induced eddy currents in highly conductive metal. Both can be reduced by building an insulating layer of H_2 [1].

The recombination rate depends on density. At the temperatures of interest in this work all recombination takes place on surface. Because of the exponential dependence of the surface density on T, even relatively small changes in the temperature can change the recombination type and rate. Decreasing the wall temperature from 200 mK to 100 mK in a sample containing equal populations of a and b atoms will destroy nearly all the a-atoms in a few seconds. If the sample is doubly polarized, at the temperature of 100 mK and bulk density of $10^{14}\,\mathrm{cm}^{-3}$ three-body recombination of b-atoms becomes dominating.

2 Magnetic resonance of hydrogen atom

2.1 Transition rules and transitions

Unlike in optical spectroscopy where electric dipolar interaction is responsible for the transitions, in ESR and NMR one has to consider magnetic interaction which is much weaker. Transitions are induced by a RF field, resonant with the transitions between the Zeeman states.

In perturbation theory the transition probability P between states $|m_S^i, m_I^i>$ and $|m_S^f, m_I^f>$ caused by the perturbation Hamiltonian $\hat{\mathbf{H}}'$ is given by

$$P \propto \left| \left\langle m_S^i, m_I^i \left| \hat{\mathbf{H}}' \right| m_S^f, m_I^f \right\rangle \right|^2 .$$

For nuclear and electron spin transitions the perturbation is

$$\hat{\mathbf{H}}' = \left(g_e \mu_B \hat{\mathbf{S}} + g_n \mu_n \hat{\mathbf{I}} \right) \cdot \mathbf{B_1}$$

where $\mathbf{B_1}$ is the amplitude of the oscillating RF magnetic field.

A transverse excitation $\mathbf{B_1} \perp \mathbf{B}$ causes single electronic and nuclear transitions. The selection rules for the electron spin transitions are $\Delta m_S = \pm 1$ and $\Delta m_I = 0$. The possible electron spin transitions are $a-d$ and $b-c$. These are studied in ESR. Selection rules for nuclear spin transitions are $\Delta m_S = 0$ and $\Delta m_I = \pm 1$. Possible transitions studied in NMR are $a-b$ and $c-d$. Possible ESR and NMR transitions are showed in figure 5 and are listed in table 2.

A parallel excitation $\mathbf{B_1} \parallel \mathbf{B}$ causes a mixed transition with simultaneous flip of electron and nuclear spins. Selection rules are $\Delta m_S = 1$ and $\Delta m_I = 1$ and the allowed transition is $a - c$.

Table 2: Allowed ESR and NMR transitions.

Transition	Δm_S	Δm_I	Type
$a-d$	± 1	0	Electron
$b-c$	± 1	0	Electron
$a-b$	0	± 1	Nucleus
$c-d$	0	± 1	Nucleus

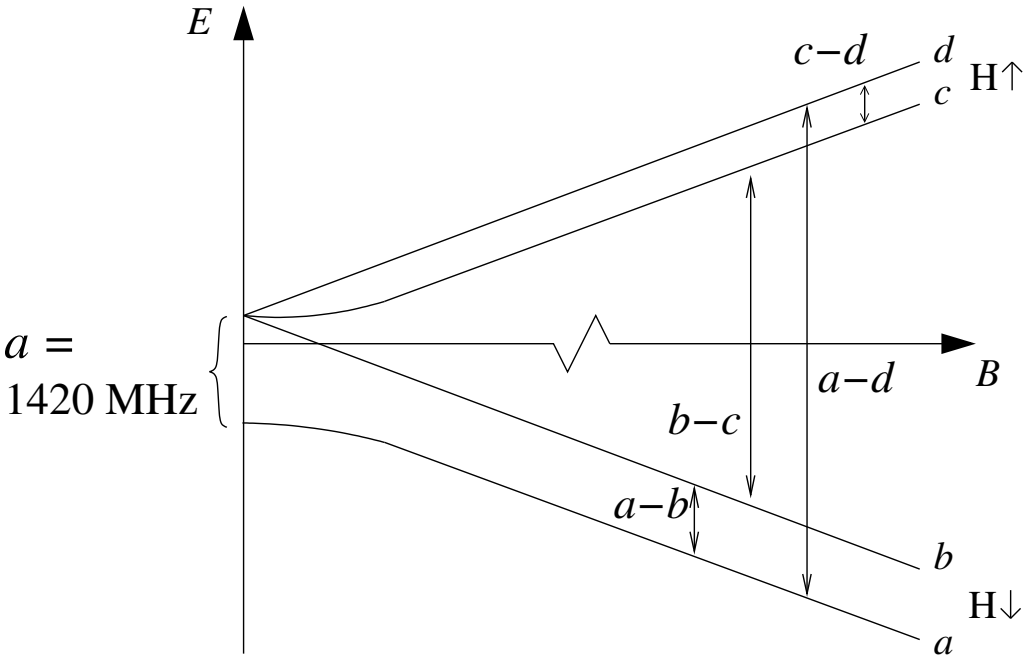

Figure 5: Possible transitions between the hyperfine energy levels.

2.2 Transition frequencies

The transition frequencies are obtained by calculating the energy differences from equations (5)-(10). The ESR transition frequencies are

$$f_{ad} = \frac{1}{2}\frac{a}{h} + \frac{1}{2}\frac{\mu^- B}{h} + \frac{1}{2}\frac{a}{h}\sqrt{1+\left(\frac{\mu^+ B}{a}\right)^2} \tag{12}$$

$$f_{bc} = -\frac{1}{2}\frac{a}{h} + \frac{1}{2}\frac{\mu^- B}{h} + \frac{1}{2}\frac{a}{h}\sqrt{1+\left(\frac{\mu^+ B}{a}\right)^2} \tag{13}$$

and the NMR frequencies

$$f_{ab} = \frac{1}{2}\frac{a}{h} - \frac{1}{2}\frac{\mu^- B}{h} + \frac{1}{2}\frac{a}{h}\sqrt{1+\left(\frac{\mu^+ B}{a}\right)^2} \tag{14}$$

$$f_{cd} = \frac{1}{2}\frac{a}{h} + \frac{1}{2}\frac{\mu^- B}{h} - \frac{1}{2}\frac{a}{h}\sqrt{1+\left(\frac{\mu^+ B}{a}\right)^2}. \tag{15}$$

The frequency of the mixed transition $a - c$ is

$$f_{ac} = \frac{a}{h}\sqrt{1+\left(\frac{\mu^+ B}{a}\right)^2}. \tag{16}$$

It is useful to compare the contributions of the hyperfine and Zeeman terms in the transition frequency. In a field of 5 T the ESR and NMR transition frequencies composed approximately of the Zeeman term and the hyperfine term:

$$\begin{aligned} g_e\mu_B B &= 140\,\text{GHz} && \text{ESR Zeeman term} \\ a/2 &= 710\,\text{MHz} && \text{hyperfine term} \\ g_n\mu_n B &= 210\,\text{MHz}. && \text{NMR Zeeman term} \end{aligned}$$

In the case of ESR the electron Zeeman term dominates. On the contrary, in NMR the hyperfine term is 3.5 times larger that the Zeeman one. Therefore, the effects of the hyperfine interaction change caused by different environments around atoms are typically studied by NMR or electron-nuclear double resonance (ENDOR) methods.

2.3 Magnetic resonance methods

2.3.1 Continuous wave and pulsed method

There are two methods used in magnetic resonance spectroscopy: Pulsed method and continuous wave (CW) method. Pulsed method is more informative, it allows to measure relaxation times more easily. Requirement to observe resonance transitions is that there has to be a population difference between the energy states.

In a classical consideration the pulsed method is based on the detection of the coherent behavior of magnetic moments after the pulse. Before the pulse magnetic moments of the sample are pointing along the polarizing field B_0. At the pulse a resonant alternating magnetic field B_1 perpendicular to B_0 is applied. In the frame rotating with the magnetic moments (Larmor rotation $\omega_L = g\mu B_0$), the excitation field creates a torque on the magnetic moments of the atoms, which leads to a coherent rotation of the magnetization around the $\mathbf{B}_1$ vector (Rabi rotation $\omega_R = g\mu B_1$). The pulse results in an excess magnetization which precesses around B_0 and induces emf to resonator which will be detected. In time, depending on the relaxation time of the substance, the precession decays and the magnetic moments align parallel to B_0. The recorded emf is called free induction decay (FID) and its Fourier transform gives the line shape which can be obtained with CW methods [16].

In the CW method either the frequency or the magnetic field is swept through the resonance. The sample is placed in a RF resonator, and a change of the oscillation amplitude and frequency in it gives an absorption and dispersion resonance lines. In the CW method magnetic field modulation is usually combined with lock-in detection to increase sensitivity. Then the derivative of the spectrum is recorded [16].

The origin of sensitivity difference between the NMR and ESR methods is in the strength of the interactions of nucleus and electron with the magnetic field. This can be seen in differences of the ESR and NMR frequencies at the same B_0. For the ESR

and NMR transition frequencies we have $f_{ESR} = g_e \mu_B B$ and $f_{NMR} = g_n \mu_n B$ and the ratio is $f_{ESR}/f_{NMR} = g_e \mu_B / (g_n \mu_n) \approx 658$. The ESR quanta have much more energy and therefore they are easier to detect than the NMR quanta. In practice the detection sensitivity can be proportional to f^3 or even f^4 [18] instead of f. The best NMR spectrometers used for studies of H can detect 9×10^{13} atoms [19]. The ESR spectrometer used in the present work has sensitivity of 10^9 atoms at excitation power of only 20 pW.

2.3.2 ENDOR

Electron-nuclear double resonance (ENDOR) can be used to study substances where both electron and nuclear magnetic moments are non-zero. In this method ESR is used to detect induced NMR transition. For NMR the effects of hyperfine interactions are more pronounced, and ESR allows high sensitivity detection [15, 16].

To illustrate the use of ENDOR, we apply it to isolated H atoms, they cannot move and they do not recombine. We detect applied the NMR $a - b$ transition from a change in the $a - d$ or $b - c$ transition ESR signal (figure 5 on page 12). First the magnetic field sweep is stopped at the ESR transition and it is saturated, so the ESR signal is zero. The ESR signal is recorded as a function of the NMR frequency. Then we start to sweep the NMR frequency over $a - b$ transition. At the NMR transition a- and b-state populations change and the saturation of the ESR transition is broken and a change in the ESR signal is detected. Complex structures of hyperfine interactions can be resolved with this method.

2.3.3 Thermal detection of magnetic resonance transitions in H↓

Unique nature of atomic hydrogen gas makes it possible to observe an induced transition by a different way. Flipping the electron/nuclear spins by ESR/NMR creates more reactive spin-up/mixed a-states which quickly recombine. The energy released in the recombination is 52000 K, which is nearly 10^4 times larger than the ESR photon energy of 7 K in the field of 4.6 T and 10^7 times larger than the NMR

quantum energy. The recombination energy can be easily detected calorimetrically. However for the ESR detection this method turned out to be less sensitive than conventional heterodyne technique [20].

In a pure b-state sample the NMR transition converts atoms to the more reactive mixed a-state. At low enough temperature, a-state atoms will recombine within seconds or tenths of seconds, compared to lifetime of the b-state atoms which is thousands of seconds. In similar way as with ESR, a sensitive bolometer can be used to detect the recombination power [20]. Difference to ESR is that a atoms recombine more slowly, which limits the speed how fast CW spectra can be recorded. There is no sensitivity difference between calorimetrically (thermally) detected ESR and NMR, because the recombination energy released after the absorption of a single photon is the same.

3 Effects of the environment of H on magnetic resonance

In our experiments we can detect H atoms simultaneously in three different systems: 1. Free atoms in the bulk gas, 2. 2D gas of atoms on the surface of LHe, 3. Atoms inside a solid H_2 layer deposited on the walls of the sample cell.

3.1 Bulk H↓ gas

The main feature of the 3D bulk gas is that the atoms are free, interactions with the wall and with each other can be neglected in the considered range of density and temperature.

A basic application of CW ESR to H↓ gas is to determine the hyperfine state a and b populations. Pulsed ESR in this gas is technically very difficult as it would lead to rapid recombination of the flipped atoms and to very short FID times. The CW lines are typically inhomogeneously broadened, and the amplitude and area of the ESR absorption peak at a low density are linearly proportional to the density of the sample. Calibration of the ESR signal against the sample density has to be done by an other method, e.g by integrating the total recombination power released during the decay of the sample [7]. First experiments on H↓ gas were done by van Yperen *et al.* [21] and Statt *et al.* [22]. Later it has been used in Moscow [23] and in Turku [20].

By NMR one can measure and manipulate the difference in $a - b$ populations. Yurke *et al.* [9] and Safonov *et al.* [10] used NMR to saturate the $a - b$ transition either to prepare the initial condition to study the recombination of the sample or to keep the a and b level populations equal through the whole sample decay. This was done to make the determination of recombination rate constants more reliable. Yurke [9] also made pulsed NMR experiments and detected FID of H↓gas. Later Johnson *et al.* [8] used pulsed NMR to detected nuclear spin waves in H↓ gas [8].

3.2 H↓ gas adsorbed on liquid helium

The main feature of H↓ adsorbed on LHe is, that there atoms are much closer to each other and to helium atoms than in bulk. The distance of adsorbed gas layer from the helium surface is 0.5 nm and the mean distance of adsorbed atoms at density $\sim 10^{12}\,\mathrm{cm}^{-2}$ is 10 nm. In comparison, in bulk at high density $\sim 10^{15}\,\mathrm{cm}^{-3}$ mean distance of the atoms is 100 nm. Interactions of the atoms with each other and with the wall should therefore be taken into account.

3.2.1 Wall shift

Binding of H atoms on He surface leads to a distortion of its electron cloud. This leads to a change in the hyperfine interaction (equation (2)). The resulting change of the zero-field hyperfine frequency, $\delta = a_{wall} - a$ is referred to as the wall shift. The wall shift in a nonzero field is expected to reflect the anisotropy of the hyperfine interaction [19].

Wall shift has been studied experimentally with different setups. In the field of 7.62 T and the surface being parallel to the magnetic field the measured value of the hyperfine interaction constant change is $\Delta a = -22.4\,\mathrm{kHz}$. The value extrapolated to zero field is $\delta = -43.2\,\mathrm{kHz}$ [19]. Zero-field measurements yielded value $\delta = -49\,\mathrm{kHz}$ [24].

From equation (13) we can calculate an estimate $\sim -0.01\,\mathrm{G}$ for the wall shift in the ESR. Typical ESR line widths are $\sim$ 0.2 G, so the wall shift is well below our ESR resolution. The case with NMR $a - b$ transition is completely different. Hyperfine interaction term in transition frequency equation $f_{ab} \approx -\frac{1}{2}\frac{a}{h} + g_n\mu_n B/h$ at 5 T is nearly three times larger than the Zeeman part. This makes even small changes in a easily visible in the spectrum. A -20 kHz change in a corresponds to shift $\sim +3\,\mathrm{G}$ from the bulk line towards higher magnetic field. This could be easily resolved from the spectrum.

3.2.2 Dipolar shift

Another type of frequency shift originates from the magnetic moments of the atoms. On the surface atoms are much closer to each other than in bulk, so the net dipolar field created by adsorbed atoms is much larger. Due to the anisotropic nature of the dipolar interaction, the corresponding frequency shift depends on the orientation of the surface to the polarizing field. Dipolar field of the adsorbate depends linearly on the surface density [26, 7]. Because of its nature, the dipolar shift is equal for ESR and NMR transitions.

The first observation of H gas on LHe surface by ESR was done in 1985 at the University of British Columbia in Vancouver [25]. They were able to see satellite lines of 2D H gas, but due to an instability of the surface lines caused by too high ESR power [7], more accurate studies were not possible [26]. The recent development in cryogenic ESR spectrometers has made possible more precise studies of 2D H gas. The maximum reached surface densities have been $\sim 5 \times 10^{12}\,\mathrm{cm}^{-2}$ corresponding to a shift of 5 G in ESR spectra. The maximum shifts of NMR line taking the wall shift into account would be around 8 G.

3.3 Hydrogen atoms in solid H_2

The main feature of this system is the interaction of H atom with the host nuclei of the H_2 lattice.

In solid H_2 impurity H atoms are under the influence of the host nuclei. The internal field generated by the nuclear magnetic moments may decrease the hyperfine interaction of H atoms, which in ESR spectrum would narrow the gap of the $a - d$ and $b - c$ lines. This effect is studied experimentally in sections 4.6–4.8.

There is also a hyperfine interaction of H electron with the nuclear magnetic moments of the lattice, which it is called the superhyperfine interaction. Like the hyperfine interaction of H atom, it is caused by the non-zero probability of the H atom electron to exist at the nuclei of the surrounding lattice. It may split the ESR

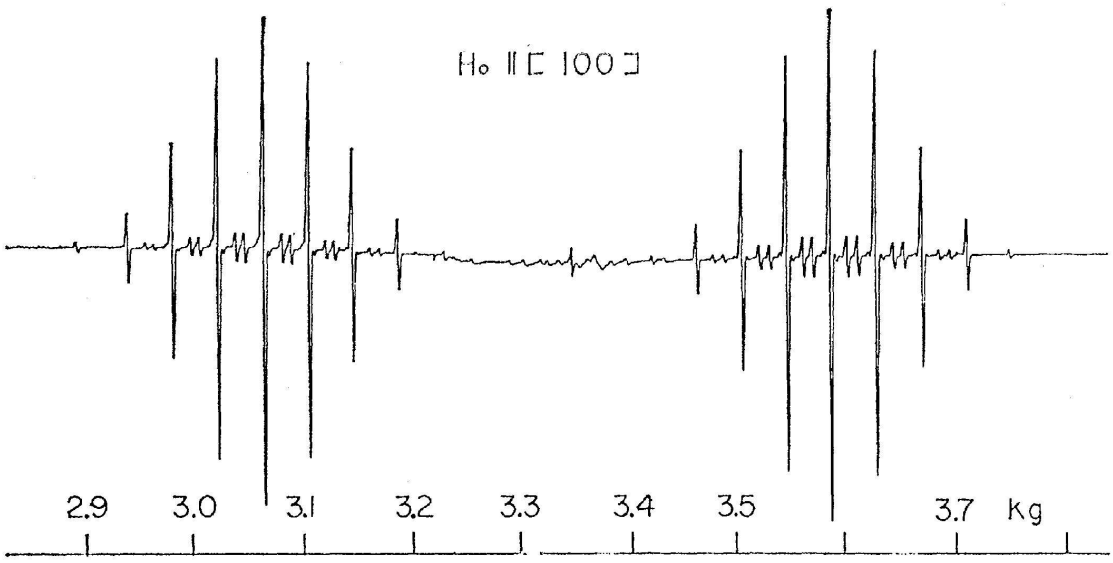

Figure 6: $b - c$ and $a - d$ ESR lines absorption derivative spectra of H atoms in CaF_2 [27].

lines to several components corresponding to different orientations of the nuclear spins in the lattice. For example, similar effects were observed in H atoms in CaF_2 (figure 6).

The hyperfine interaction change will be much more pronounced in the NMR and ENDOR than in ESR spectra. The shape and structure of the magnetic resonance lines contain information on the position of the atoms in the lattice, and on the quality of the crystal. In disordered solids the NMR and ENDOR lines do not have any structure, but are broadened due to a random distribution of the internal field experienced by the atoms. It is very important to know how good are the H_2 crystals in order to evaluate the possibility of rapid tunneling motion of the atoms along the crystal.

4 Experiments and results

4.1 Experimental setup

The present experiments were conducted in the Wihuri Physical Laboratory of the University of Turku. The experimental setup, constructed for the studies of H$\downarrow$ gas, includes a cryostat with a dilution refrigerator which can reach 30 mK and an ESR spectrometer operating at 128 GHz. Recently a NMR resonator was added to the setup.

H gas is created in a cryogenic dissociator operating at $\sim$0.7 K. The atoms are pulled from the dissociator to the sample cell (SC) by a field gradient. Dissociator is cooled by a separate ^{3}He refrigerator which has a much higher cooling power than is available from the dilution refrigerator [28].

The main polarizing magnetic field of 4.6 T is generated by a superconductive magnet working in persistent mode. The fine tuning of the field and the magnetic field sweeps used in ESR and NMR are done with a separate sweep coil, which operates in the range $\pm 570\,\mathrm{G}$.

The ESR spectrometer works in the CW mode and is of heterodyne type, which allows simultaneous detection of absorption and dispersion signals [28]. In experiments the mm-wave excitation frequency is kept constant and the magnetic field is swept through the resonance [28].

Experiments with H$\downarrow$ gas are carried out in the SC, where the ESR and NMR resonators are located (figure 7). The upper part of the ESR resonator, isolated by a thin Mylar foil from the rest of the sample cell, is filled with coolant taken from the mixing chamber of the dilution fridge. With this method the central part of the Mylar foil, called Cold Spot (CS), can be cooled substantially below the temperature of the rest of the SC (figure 8). CS is used to thermally compress 2D H$\downarrow$ gas adsorbed on LHe film [29]. With this method it is possible to get high densities, $\sigma \sim 5 \times 10^{12}\,\mathrm{cm}^{-3}$ for the 2D atomic hydrogen gas and to study each sample at the time scale of several hours [2, 29].

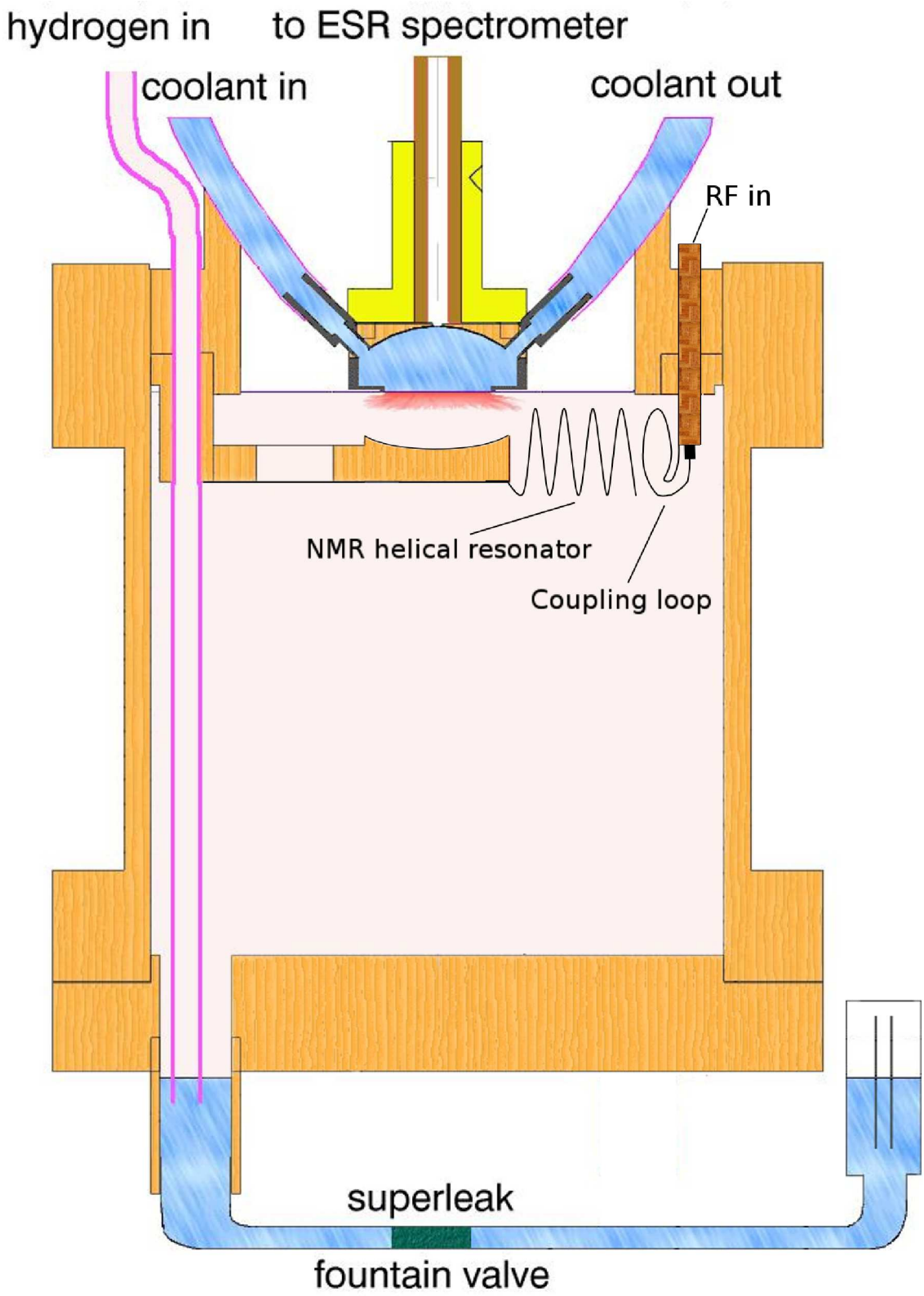

Figure 7: Sample cell with ESR and NMR resonators.

The ESR resonator is of the Fabry-Perot (FP) type and consists of two spherical mirrors. It operates in the TEM_{006} mode and has $Q \sim 2000$ at $f \approx 128\,\mathrm{GHz}$. The operating frequency of the FP resonator f_{FP} is defined by the tuning range of the ESR spectrometer $f_{ESR} = 128 \pm 0.5\,\mathrm{GHz}$ [28]. This is a relatively narrow frequency range, taking into account that cooling down the resonator from room temperature to LHe changes its frequency by $\approx +1.5\,\mathrm{GHz}$, and filling with the coolant decreases f_{FP} by $\approx -2.5\,\mathrm{GHz}$. Therefore, these shifts were measured in preliminary cooldown tests, and were taken into account in the final tuning of the resonator at room temperature. Since ESR is the main detection tool, its sensitivity is of prime importance. Therefore the FP resonator is designed to have the highest possible Q-value, and the final operating frequency of the ESR is set by the FP resonator at real conditions of the experiment. The millimeter-wave field inside the resonator is a standing wave having seven maxima, four of which are are used to detect H gas (figure 8). Other maxima are located in the coolant volume. The Mylar foil divides the FP resonator in to two equal parts. The lower one is filled by H$\downarrow$ bulk gas. 2D H$\downarrow$ sample is adsorbed on the lower surface of the foil and is located in the maximum of the millimeter-wave field.

Once the ESR operating frequency (f_{ESR}) is set, it defines resonance fields B_{ad} and B_{bc} for the $a-d$ and $b-c$ transitions (separated by 507 G). The corresponding change in the NMR transition frequency is $\approx 2\,\mathrm{MHz}$. Therefore, in order to be able to excite the NMR transition simultaneously with either $a-d$ or $b-c$ ESR lines, the width of the NMR resonator should be $\gtrsim 2\,\mathrm{MHz}$. This means that the NMR resonator Q should be $\lesssim 500$. A low Q value makes also the frequency tuning much easier. It would be desirable to get the NMR resonator maximum to the $a-b$ transition frequency corresponding to the B field in the middle of the $b-c$ and $a-d$ ESR lines.

The NMR resonator consists of a coupling loop and a resonant helix. The coupling loop is connected to the end of a coaxial cable leading to room temperature and RF source. The resonant helix is inductively coupled to the coupling loop and

operates in the $\lambda/4$ mode [30, 9] (figure 7). Tuning of the NMR resonator has to be done also at room temperature. Surroundings can influence its operating frequency easily by 50 MHz, so the final tuning must be done when the resonator is installed in the SC.

The NMR resonator frequency change due to cooling was measured separately. Pumping the resonator to high vacuum increased its frequency by $\sim 1\,\mathrm{MHz}$ and cooling to 4 K increased the frequency by another $\sim 7\,\mathrm{MHz}$. Filling the CS with coolant didn't influence the frequency. The desired frequency at the experimental conditions was achieved within an accuracy of 1 MHz. A coarse tuning of the NMR resonator frequency was done by changing the resonant helix wire length. Fine tuning was done by changing the capacitance between the helix turns by adjusting the separation between the resonant helix turns.

In our experimental conditions the NMR resonator operates at 908 MHz and the width of its resonance is $\approx$2 MHz. In NMR experiments either magnetic field or frequency can be swept. In the present measurements we use the field sweep. An induced NMR transition in H$\downarrow$ gas is detected from recombination heat by a temperature controller (TC), which stabilizes the SC temperature. Changes of the feedback power of the TC are equal to the recombination heat generated in the SC [28]. ESR or NMR induced recombination can be easily detected by this method. Compared to the bolometer detection this method has a much larger time constant and requires very slow sweeps $\gtrsim 500\,\mathrm{s}$.

In typical experiments with H$\downarrow$ gas, the sample is first loaded to the cell by running the dissociator for about an hour. During the accumulation of the sample, the cell is kept relatively warm at $\sim 200{-}300\,\mathrm{mK}$ in order to decrease recombination. After reaching the saturated density, the dissociator is turned off, the cell is stabilized to a desired temperature, typically to $\sim$170 mK, and the CS is cooled down to temperatures below 100 mK. The decay of the H$\downarrow$ sample is monitored by ESR and TC.

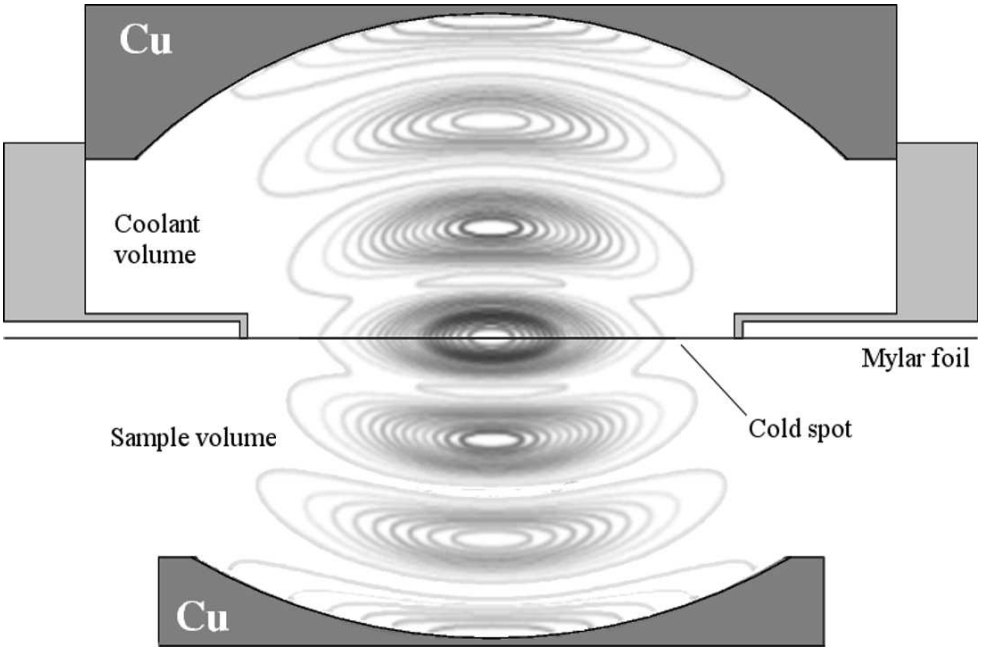

Figure 8: Excitation field inside the ESR resonator. No ESR signal originates from the upper volume filled with coolant. In the lower volume there are two field maxima on the surfaces, where 2D H and H_M gas can be detected. In practice the 2D H gas on the spherical Cu mirror is not visible in the ESR spectra.

4.2 Approximate transition frequencies of H↓

The operating magnetic field in the experiments is defined by the ESR frequency, so it is useful to give the $a-b$ NMR frequency as a function of the ESR frequency f_{ESR}. The ESR $b-c$ and $a-d$ transition frequencies as a function of the magnetic field are plotted in figure 9.

The resonance magnetic fields as a function of the excitation frequency f_{ESR} can not be explicitly solved from equations (12) and (13). Those can be calculated numerically, or in a high field when $\frac{\mu^+ B}{a} \gg 1$, the approximation

$$\frac{1}{2}\frac{a}{h}\sqrt{1+\left(\frac{\mu^+ B}{a}\right)^2} \approx \frac{1}{2}\frac{\mu^+ B}{h} \tag{17}$$

can be used to simplify the transition frequency equations. From the exact transition frequency equations (12) and (13) with this approximation we obtain

$$f_{ESR}(B_{bc}) \approx -\frac{1}{2}\frac{a}{h} + \frac{g_e\mu_B B_{bc}}{h} \quad (18)$$

$$f_{ESR}(B_{ad}) \approx +\frac{1}{2}\frac{a}{h} + \frac{g_e\mu_B B_{ad}}{h}. \quad (19)$$

In the field of $B = 4.6\,\mathrm{T}$ equations (18) and (19) give $\sim 4\,\mathrm{MHz}$ too low values, which is neglible compared to 128 GHz.

From equations (18) and (19) we get $B_{bc}(f_{ESR})$ and $B_{ad}(f_{ESR})$ in an explicit analytical form,

$$B_{bc}(f_{ESR}) \approx \frac{hf_{ESR} + \frac{1}{2}a}{g_e\mu_B} \quad (20)$$

$$B_{bc}(f_{ESR}) \approx \frac{hf_{ESR} - \frac{1}{2}a}{g_e\mu_B}. \quad (21)$$

These approximate equations give $1.4\,\mathrm{G}$ too large values at $4.6\,\mathrm{T}$.

When calculating the NMR frequency as a function of ESR frequency, it is practical to use the approximate NMR transition frequency calculated from equations (6) and (7)

$$f_{ab}(B) \approx \frac{1}{2}\frac{a}{h} + \frac{g_n\mu_n B}{h} + \frac{h(a/h)^2}{4\mu^+ B}. \quad (22)$$

For $B = 4.6\,\mathrm{T}$ equation (22) gives about $120\,\mathrm{Hz}$ too large value. In magnetic field it corresponds to $-0.02\,\mathrm{G}$, which is well below the resolution of our measurements. A NMR transition frequency change of $4.2\,\mathrm{kHz}$ shifts the line position in field by $\approx 1.0\,\mathrm{G}$.

Now we can write down $f_{ab}(\,B_{bc}(f_{ESR})\,)$:

$$f_{ab}(f_{ESR})|_{bc} \approx \frac{1}{2}\frac{a}{h} + \frac{g_n\mu_n}{g_e\mu_B}\left(f_{ESR} + \frac{1}{2}\frac{a}{h}\right) + \frac{(a/h)^2}{4\mu^+}\frac{g_e\mu_B}{f_{ESR} + \frac{1}{2}a/h}. \quad (23)$$

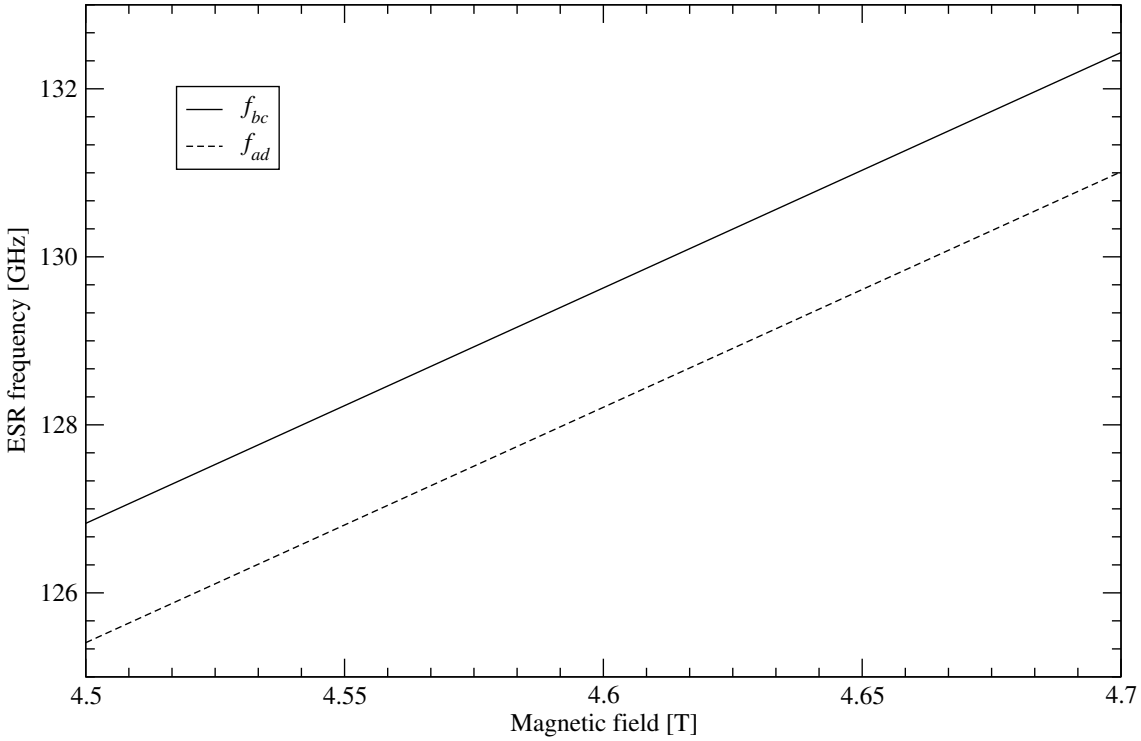

Figure 9: ESR $b-c$ and $a-d$ frequencies.

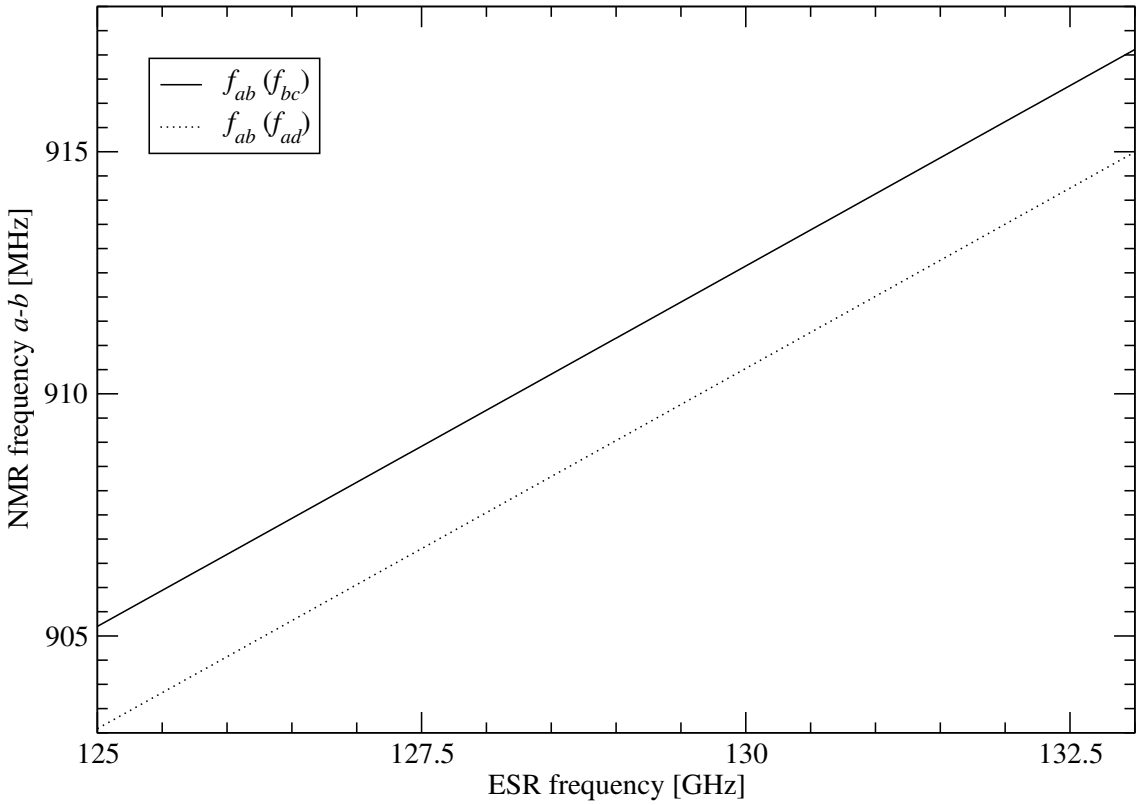

Figure 10: NMR $a-b$ frequency as a function of $b-c$ and $a-d$ ESR frequencies.

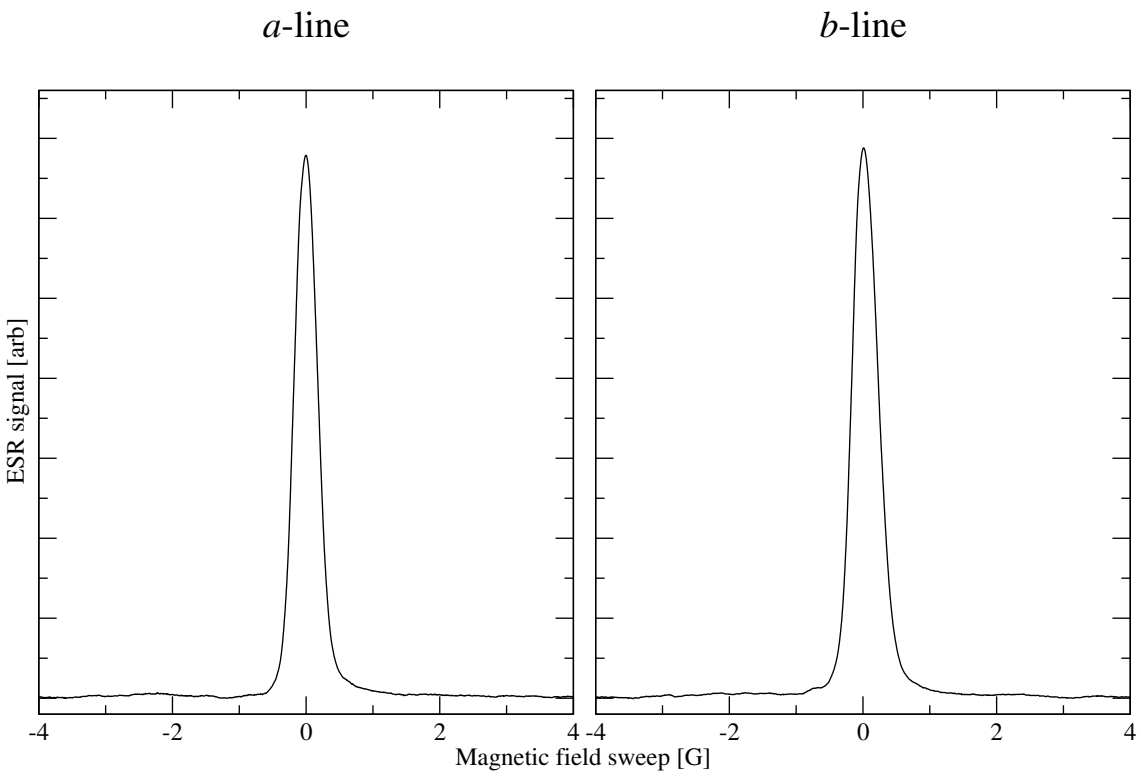

Figure 11: ESR spectra of bulk a- and b-line during the accumulation of a sample at the cell temperature $T_{SC} \approx 300\,\mathrm{mK}$. Density of the sample is $n_a + n_b \sim 10^{15}\,\mathrm{cm}^{-3}$.

4.3 ESR in bulk H$\downarrow$ gas

During the accumulation of a sample conditions are optimized to get maximum bulk density in the SC. Both a- and b-states are collected in the SC in approximately equal amounts. Spectra of a- and b-line while running dissociator are presented in figure 11. Density of the sample is $n_a + n_b \sim 10^{15}\,\mathrm{cm}^{-3}$. In a typical 2D H gas compression experiment the dissociator is switched off and SC is cooled to ~170 mK and CS below 100 mK. The decay of the sample is measured after that. Cooling the SC and/or CS to below 100 mK leads to a rapid build-up of nuclear polarization in the gas, and the a-line disappears from the spectrum.

Bulk state densities are obtained by comparing peak areas of spectra with some reference spectrum peak area, for which the density is calibrated calorimetrically. The bulk lines are broadened due to a magnetic field inhomogeneity in the FP resonator. This inhomogeneity can be reduced by the factor ~ 1.5 using an additional

shim coil mounted around the SC. In the spectra of figure 11 shim coil was used to reduce line width.

The same shim coil can be used to increase the field gradients, and selectively excite atoms in different regions of the FP resonator. This is demonstrated in figure 12. When there is no gradient applied, $I_{grad} = 0\,\mathrm{A}$, the line shape is more broad than in figure 11. After applying a current $I_{grad} = 0.2\,\mathrm{A}$ to the coil four peaks appear, each originating from different mm-wave maxima in the resonator (figure 8). The rightmost peak is from the maximum at CS and the leftmost is from the lower spherical mirror. The two larger peaks in the middle correspond to the maxima between the foil and the mirror. By applying larger gradients the peaks originating from different maxima are separated and broadened more (figure 12). The rightmost peak is narrower than other peaks because the space where H atoms are detected in the mm-wave maximum is reduced by the Mylar foil (figure 8).

The basic application of ESR is the measurement of the bulk density. We can also calculate the magnetic field precisely at bulk line place from transition frequency equations (12) and (13). By applying known magnetic field gradients in the H gas detection volume, we get information about the spatial profile of the mm-wave field in the resonator.

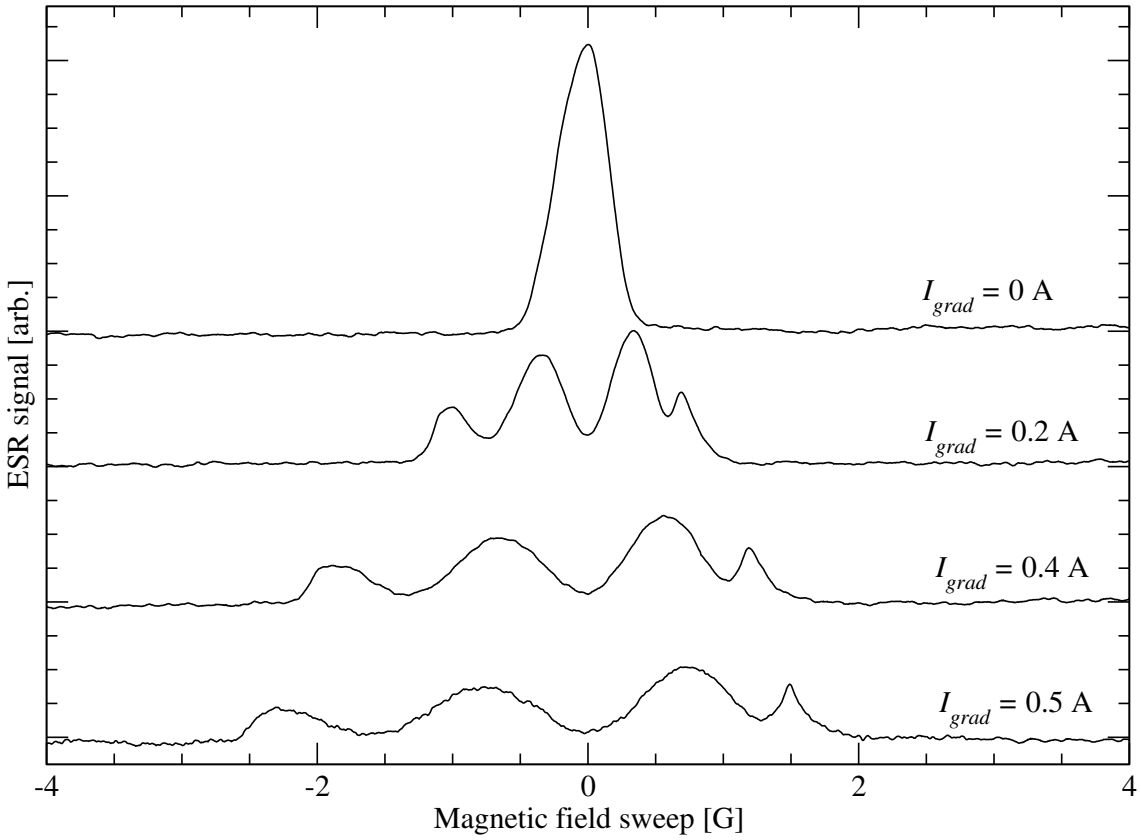

Figure 12: ESR $b - c$ bulk line for different shim coil currents I_{grad}. The applied field gradient is mainly axial.

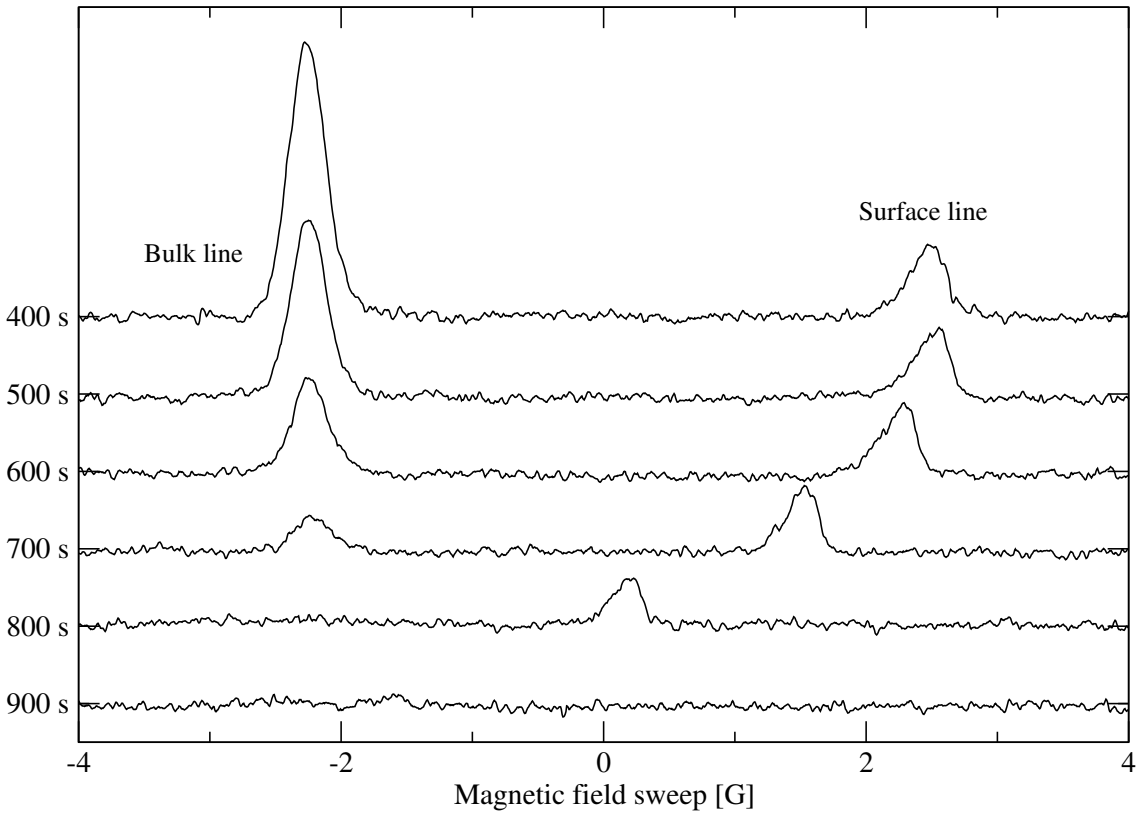

Figure 13: Time evolution of ESR $b-c$ bulk and surface lines after 400 s starting the compression. $T_{cell} \approx 200\,\mathrm{mK}$, $T_{CS} \approx 100\,\mathrm{mK}$.

4.4 2D ESR line

Activating thermal compression on the CS leads to the appearance of a second line in the ESR spectrum, shifted to the higher field from the bulk line. Cooling the CS from 200 mK to 100 mK increases surface density ~ 200 times, so much that H atoms on the surface become easily detectable by ESR. A high surface density increases the dipolar field of the adsorbed atoms. This is visible in ESR spectrum as a line shift of the surface atoms [26, 7]. The shift of the surface line from the bulk one is linearly proportional to the surface density [7].

Time evolution of the ESR absorption spectra in a CS compression experiment is presented in figure 13. Lifetime of the sample after starting compression was about $\sim 900\,\mathrm{s}$. Both bulk and surface density can be measured by calculating the integrals of the absorption lines. Slow drift of the bulk line place is linear, and is caused by a decay of the persistent current in the superconductive magnet. The surface line

shape depends on the density profile of adsorbed atoms. When the density profile is inhomogeneous, it can be extracted from the detected line shape [7].

4.5 Thermal detection of $a - b$ NMR transition in bulk H$\downarrow$ gas

To detect the recombination power in the SC one can use the feedback power of its TC or a bolometer [20]. In this work we used the first method. The main disadvantage of the TC detection is its relatively large time constant $\tau_{TC} \sim 5\,\mathrm{s}$. However, at high enough temperatures of the SC, slow recombination of a-atoms may set another limit to the overall detection time constant. Lowering the SC or CS temperature leads to a fast recombination, but reduces the lifetime of the whole sample. Therefore, we had to compromise between these things and find optimal temperature of the SC and CS. Even at these conditions we had to use a very slow sweep speed, $\sim 30\,\mathrm{s/G}$ compared to $\sim 5\,\mathrm{s/G}$ without TC detection to avoid distortions of the recorded signals. To make accurate measurement of the NMR line position we recorded it sweeping in both directions increasing and decreasing the sweep field and taking the mean value for the result. The difference in the peak positions swept in different directions was ≈ 2 G (figure 14). This procedure allows to reduce the error in the determination of the NMR line position to $\lesssim 0.5\,\mathrm{G}$.

The numerically calculated NMR transition frequency f_{ab} corresponding to $f_{ESR}|_{bc}$ is 909.289 MHz. In the experiment the SC and CS temperatures were set to $\sim 170\,\mathrm{mK}$ and the NMR frequency to 909.287 MHz. A $-2\,\mathrm{kHz}$ change in the used NMR frequency shifts observed line by $\sim 0.5\,\mathrm{G}$ to lower field. To compare the NMR line position at $f_{ab}(f_{ESR})|_{bc}$ with the ESR line position we had to add 0.5 G to the NMR line place. In figure 14 the NMR line is in the center of vertical lines corresponding to line positions measured from from different direction sweeps. From the NMR line at f_{ab} =909.287 MHz the NMR line at $f_{ab}(f_{ESR})|_{bc}$ is 0.5 G in the higher field (dotted line). From the NMR and ESR line position difference we conclude

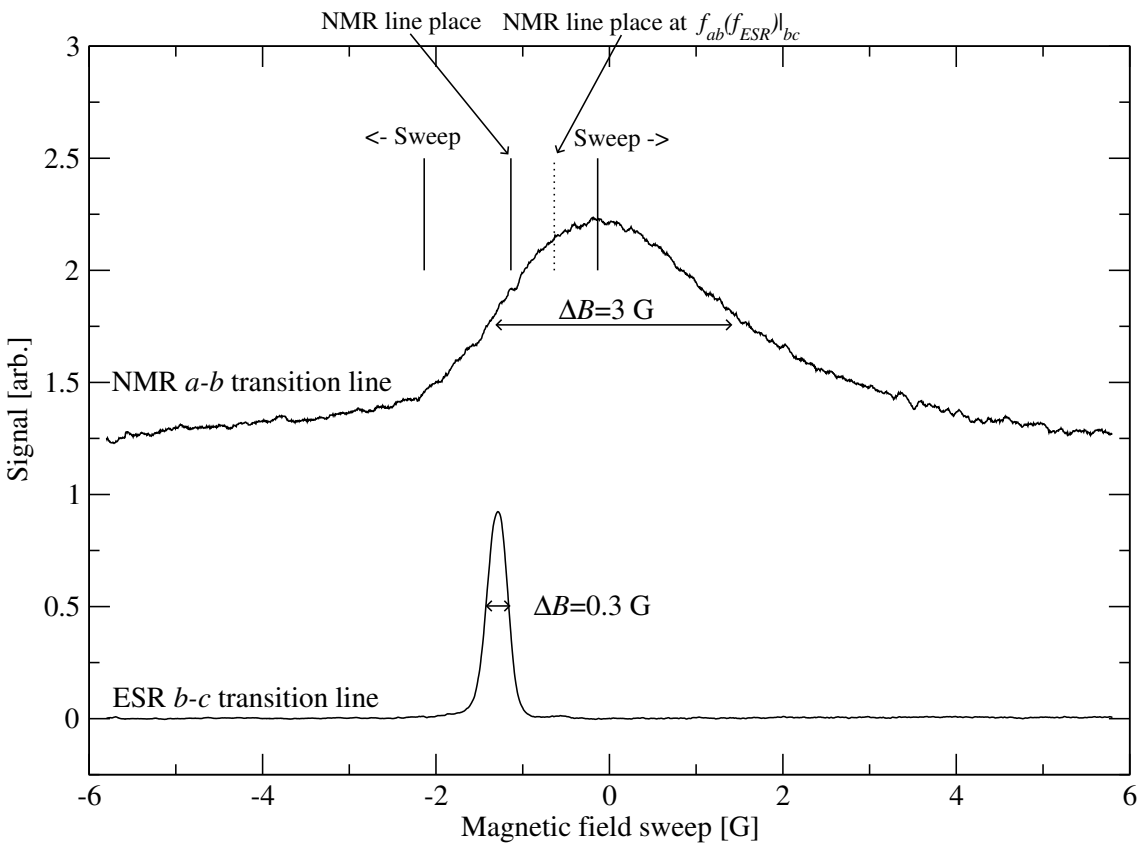

Figure 14: NMR $a-b$ and ESR $b-c$ spectra. The rightmost and leftmost vertical lines correspond to NMR line places when sweeping to different directions. The vertical line in the middle corresponds to the true line position and the dotted line line is at $f_{ab}(f_{ESR})|_{bc}$.

that the NMR resonator is in about 1 G lower field than the ESR resonator.

The large NMR line width is due to the large NMR excitation field space. The $a-b$ NMR transition in bulk H gas is mainly induced inside the NMR resonant helix (figure 7). Its width is ~ 6 mm and height ~ 5 mm, and the resonator is not in the center of the superconductive magnet, where magnetic field is most homogeneous. Unlike with the ESR, where main field inhomogeneity is axial, NMR suffers from both axial and radial field inhomogeneities and it is much more difficult to decrease the line width by applying magnetic field gradients.

From the measurements we can extract the NMR line place with an accuracy of 0.5 G. The large NMR line width ~ 3 G is due to inhomogeneous magnetic field in the area of the NMR excitation field. By comparing NMR and ESR line positions we

can measure the field inhomogeneity between the resonators. The measured value, NMR resonator being in$\sim$1 G lower field than the ESR resonator, is inside the upper limit of the field inhomogeneity given by the NMR line width $\sim 3\,\mathrm{G}$.

4.6 ESR detection of H gas in H_2

In experiments with H$\downarrow$ a layer of solid molecular hydrogen is typically grown on the walls of the SC. This is needed to reduce the rate of the $b \rightarrow a$ relaxation on the walls. The layer is formed by molecules resulting from the recombination of atoms in the SC. With the atom flux $\sim 2 \times 10^{13}\,\mathrm{s}^{-1}$ of our dissociator and the cell area of $\approx$100 cm^2 one monolayer of H_2 is built in $\sim$ 2 hours. Therefore one needs several days of continuous operation of the dissociator to build $\sim 30\,\mathrm{nm}$ thick H_2 layer comparable with the thickness of the saturated ^{4}He film. During the coating procedure we found an extra peak to appear in the ESR spectrum.

Lowering the SC temperature to 100 mK so that all H gas is destroyed in recombination, did not influence the new line. Applying an axial gradient splits the line to two components (15). Further coating increased the line strength, and the fastest growth rate was observed at the highest steady state bulk density in the SC during coating. The width of the new line was $\approx 0.7\,\mathrm{G}$ just after completing the coating, then it gradually decreased to 0.2 G in two weeks. We conclude that the new line originates from H atoms inside the H_2 layer on the lower ESR mirror and CS. Highly excited H_2 molecules give a large kinetic energy to H atoms, which allow them to penetrate though the LHe film and stick to the cell wall [11].

In figures 16-18 we present examples of the spectra of H$\downarrow$ and H_M samples for different bulk H$\downarrow$ densities. By integrating the H_M absorption lines we calculate the number of H atoms in the H_M sample. Then we can estimate the density of atoms $n_{H_M} \approx 2-3\times10^{18}\,\mathrm{cm}^{-3}$, or their relative concentration in H_2 being $5\times10^{-5}-10^{-4}$. These are much higher densities than we can reach in H$\downarrow$.

The H_M b-line is much weaker than the a-line. We found that the b-line is more

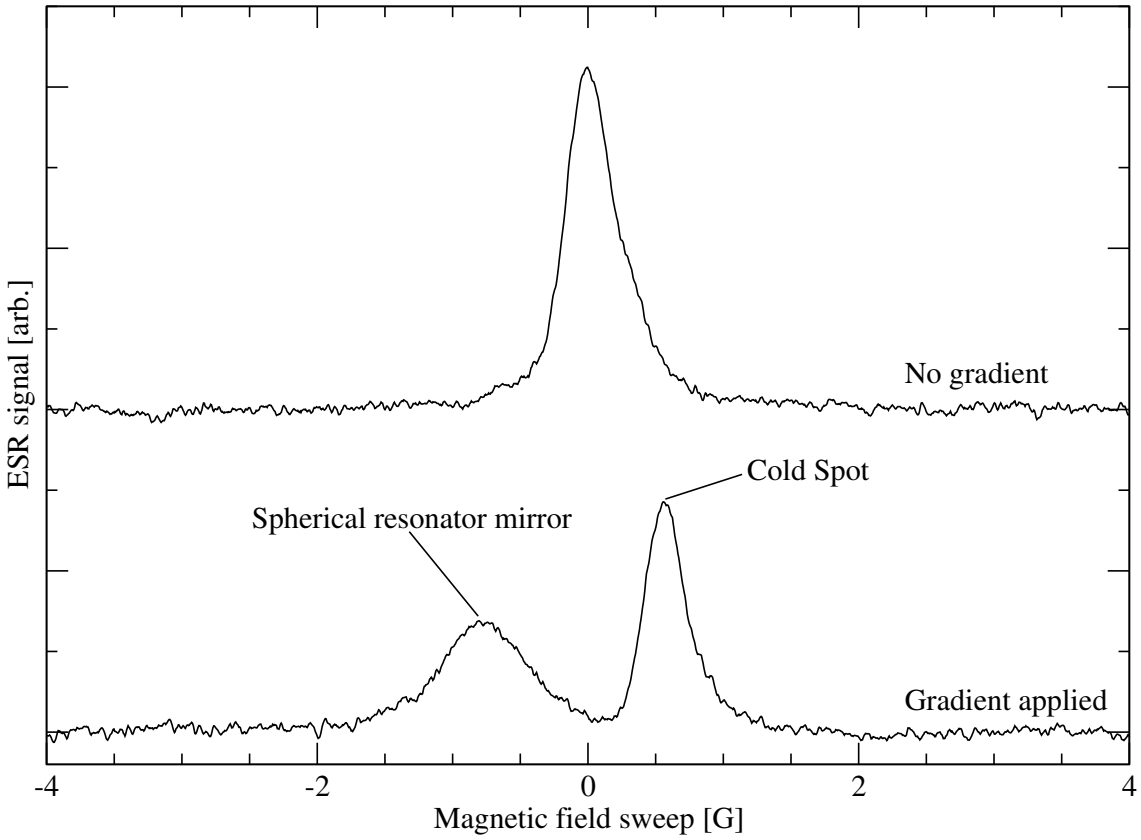

Figure 15: Axial field gradient splits ESR H_M $a-d$ line to two components which originate from the lower ESR resonator mirror and the CS.

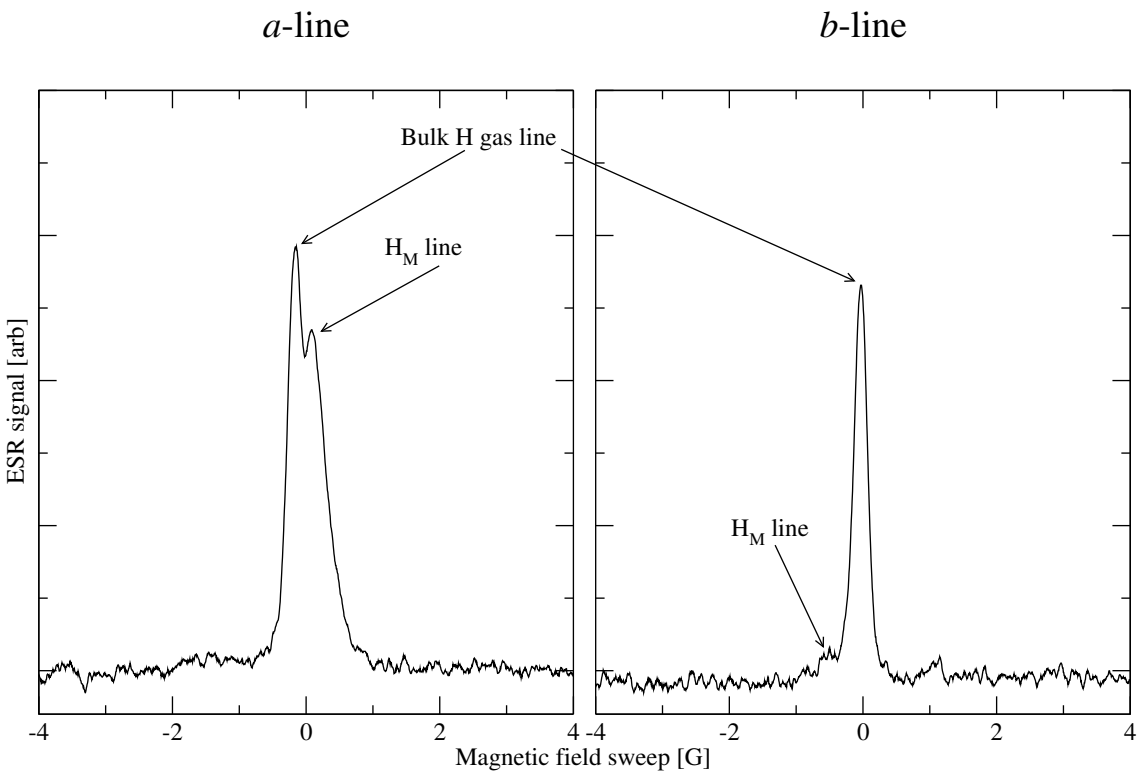

Figure 16: ESR a- and b-lines of H$\downarrow$ and H_M samples. ESR signal axis tick mark scales are the same as in figures 17 and 18.

easily saturated by ESR excitation than the a-line. Its recovery after saturation is defined by the nuclear relaxation time in the lattice, which turned out to be very long ($\sim 2-3$ days). The difference in saturation behavior of $a-d$ and $b-c$ transitions requires further studies and understanding [11].

The position of the center of ESR spectrum is defined by the g-factor as $hf = g\mu_B B$. The splitting between H $a-d$ and $b-c$ lines is caused by the hyperfine interaction $f_{bc} - f_{ad} = a$. Both H_M lines are shifted towards the center of the spectrum, which means that in $H_M$the hyperfine constant is smaller and the g-factor is very close to that of free atoms.

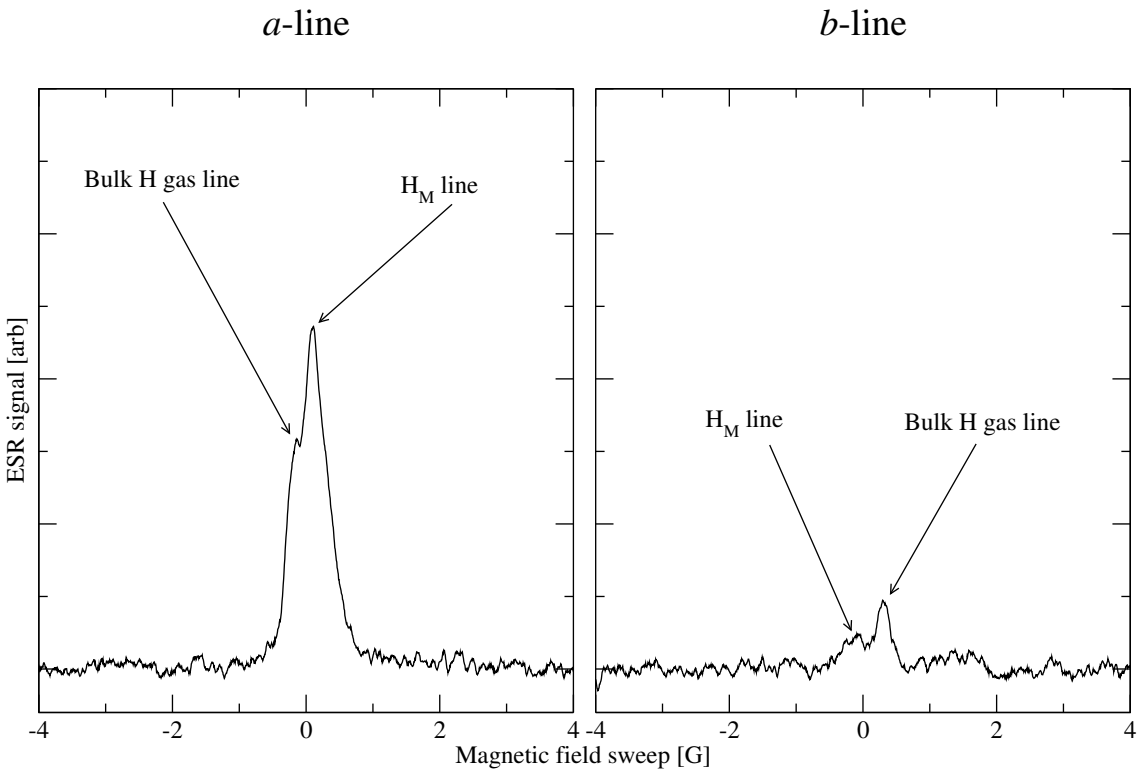

Figure 17: H_M *a*- and *b*-line with lower bulk density than in figure 16.

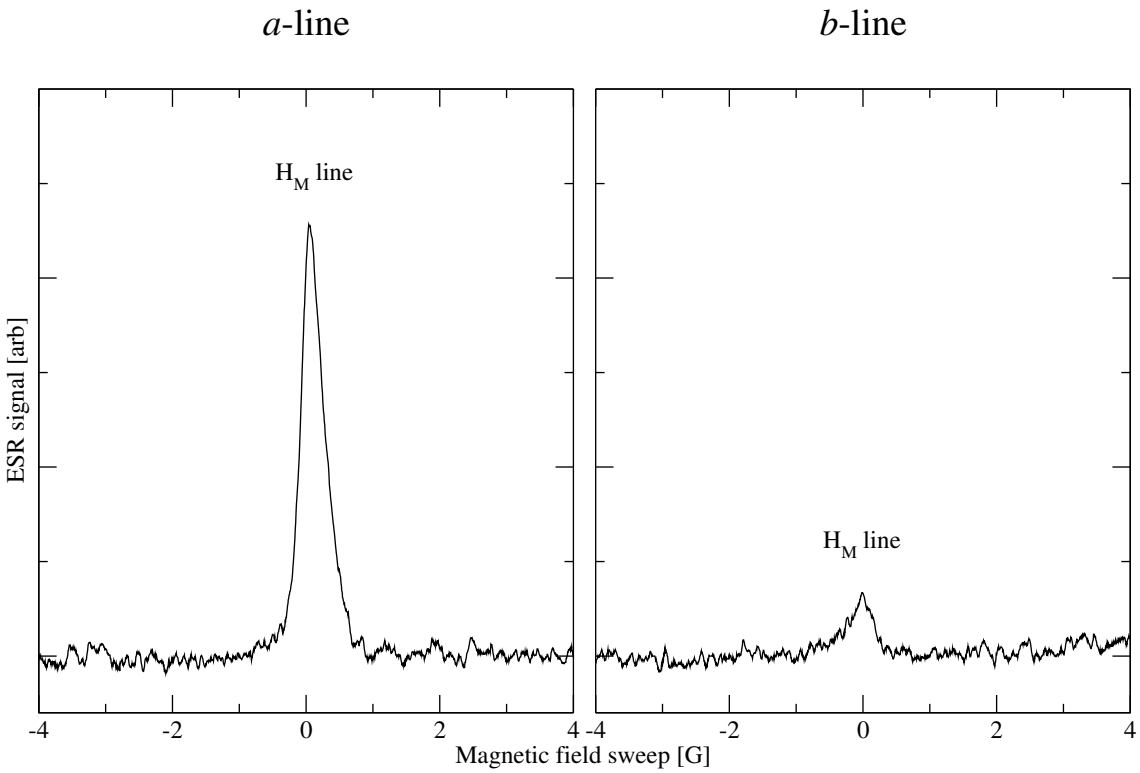

Figure 18: ESR bulk signals have disappeared and only H_M lines are visible.

4.7 ESR measurement of the hyperfine coupling constant of H atoms in solid H_2

The shift of H_M line from bulk line can be easily measured for a-line, because both lines are strong enough and are visible at the same time. H_M b-line is much weaker and cannot be resolved well when there is bulk line visible. The drift of the main field creates another problem. Therefore several b-line spectra of both H_M and bulk gas were taken, and the line positions were extrapolated in the cases when only one line was visible. The measured shift for both a- and b-line is $|\Delta B| = 0.28 \pm 0.05\,\mathrm{G}$.

Change of the hyperfine coupling constant can be calculated from the shift between H_M and bulk line. For $b - c$ transition from equation (18) we write

$$f_{bc} = -\frac{1}{2}\frac{a_0}{h} + \frac{g_e \mu_B B}{h}. \tag{24}$$

The hyperfine constant a is now marked with a_0. The change of the hyperfine constant $a_0 \to a_0 + \Delta a$ leads to the shift of the line $B \to B + \Delta B$, so that

$$f_{bc} = -\frac{1}{2}\frac{(a_0 + \Delta a)}{h} + \frac{g_e \mu_B\,(B + \Delta B)}{h}. \tag{25}$$

Solving these equations for Δa we obtain

$$\frac{\Delta a}{h} = 2 g_e \mu_B \Delta B. \tag{26}$$

For the shift of $\Delta B = -0.28\,\mathrm{G}$ obtained in the measurements we get

$$\frac{\Delta a}{h} = -1.6 \pm 0.3\,\mathrm{MHz}. \tag{27}$$

Measurement is quite inaccurate, because the shift is small compared to the ESR line width $\sim 0.2\,\mathrm{G}$.

This is the first direct measurement of the hyperfine constant change for H atoms inside solid H_2. It has not been possible to detect $H\downarrow$ and H_M lines simultaneously

in previous experiments [11, 12]. Negative sign in Δa means that the density of the electron wave function at the nucleus is reduced for H atoms in H_2 lattice. This can be explained by attraction of the electron to the neighboring H_2 molecules.

4.8 NMR pumping of $a - b$ transition in H_M

As was mentioned earlier, the effect of hyperfine interaction change is much larger for NMR than for ESR. That is why NMR and ENDOR methods are used to resolve the structure caused by interactions with the lattice. From the ESR measurements it is not possible to determine, how broad the resonance is, or are there several hyperfine states of H atoms in H_2. This is an interesting thing that we would like to find out as well. Width of the resonance depends on the quality of the crystal structure of H_2, and different positions of H atoms in H_2 lattice could be identified if the structure of the hyperfine interactions would be resolved.

Direct detection of H_M by NMR is not possible because of too low sensitivity. It could be circumvented by using ESR as the detection tool, in a similar way as what is done in ENDOR. In it, NMR transitions are detected from their's influence to strong ESR signal. Saturation of $a \rightarrow b$ transition will equalize the populations of a- and b-states. This can be detected by comparing ESR lines before and after pumping the NMR transition. Conventional ENDOR cannot be implemented due to too long $a - b$ relaxation time.

NMR frequency shift $\Delta f_{ab} = f_{ab}(a = a_0 + \Delta a) - f_{ab}(a = a_0)$ can be calculated using approximated transition frequency equation (22) and neglecting third term in it. We get

$$\Delta f_{ab} = \frac{1}{2}\frac{\Delta a}{h}. \tag{28}$$

By taking Δa obtained from the ESR line shift measurement, we get an estimate for the NMR frequency change:

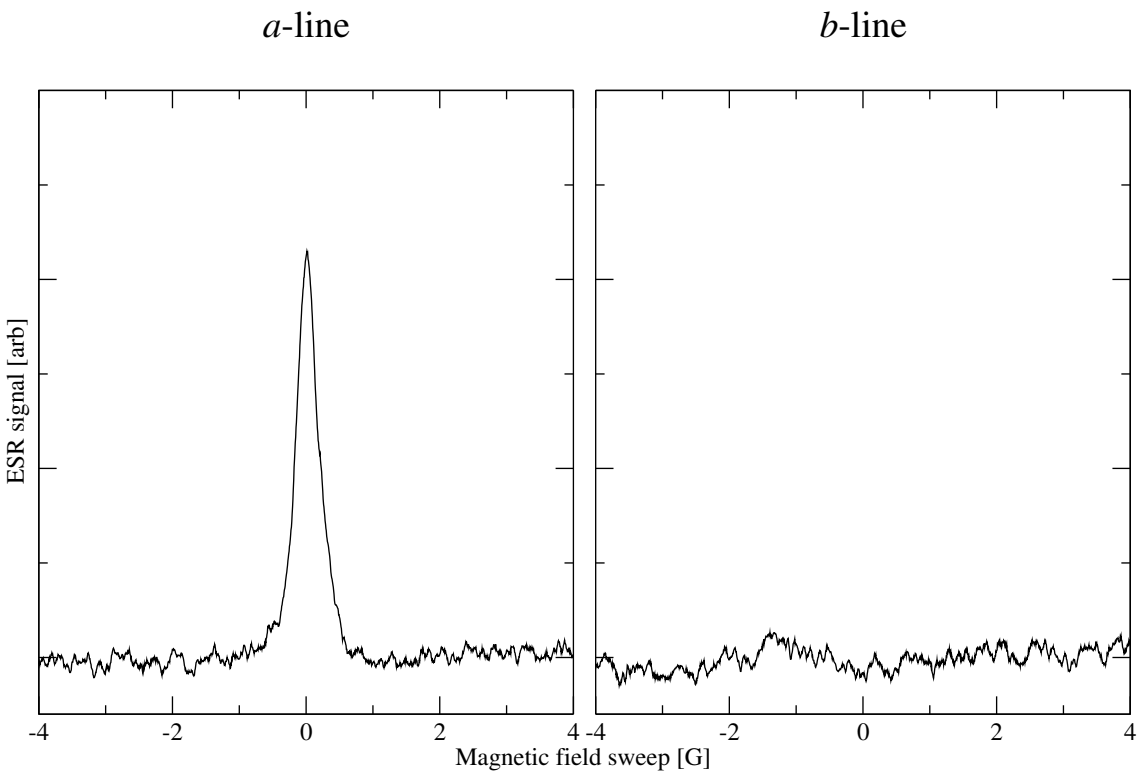

Figure 19: ESR H_M a- and b-lines before starting the NMR pumping of $a - b$ transition.

$$\Delta f_{ab} = -0.8 \pm 0.15\,\mathrm{MHz}. \tag{29}$$

In the field defined by ESR ($f_{ESR} = 127.754\,\mathrm{GHz}$) estimated $a - b$ transition frequency for H_M is

$$f_{ab\,H_M} = 908.5 \pm 0.15\,\mathrm{MHz}. \tag{30}$$

Based on the previous ESR measurements of Δa we get a rather rough estimate for the NMR H_M transition frequency. The error in our estimate 0.15 MHz is much larger than bulk $H\downarrow$ line width $\sim 12\,\mathrm{kHz}$. We do not know the width of the H_M NMR transition, just that it is something from 12 kHz to 800 kHz. Lower limit of the H_M NMR line width is set by the magnetic field inhomogeneity. Upper limit is set by the observed width of the H_M ESR line.

The experiment on pumping the $a - b$ transition in H_M was started with the a- and b-populations represented in figure 19. There is no visible population in the

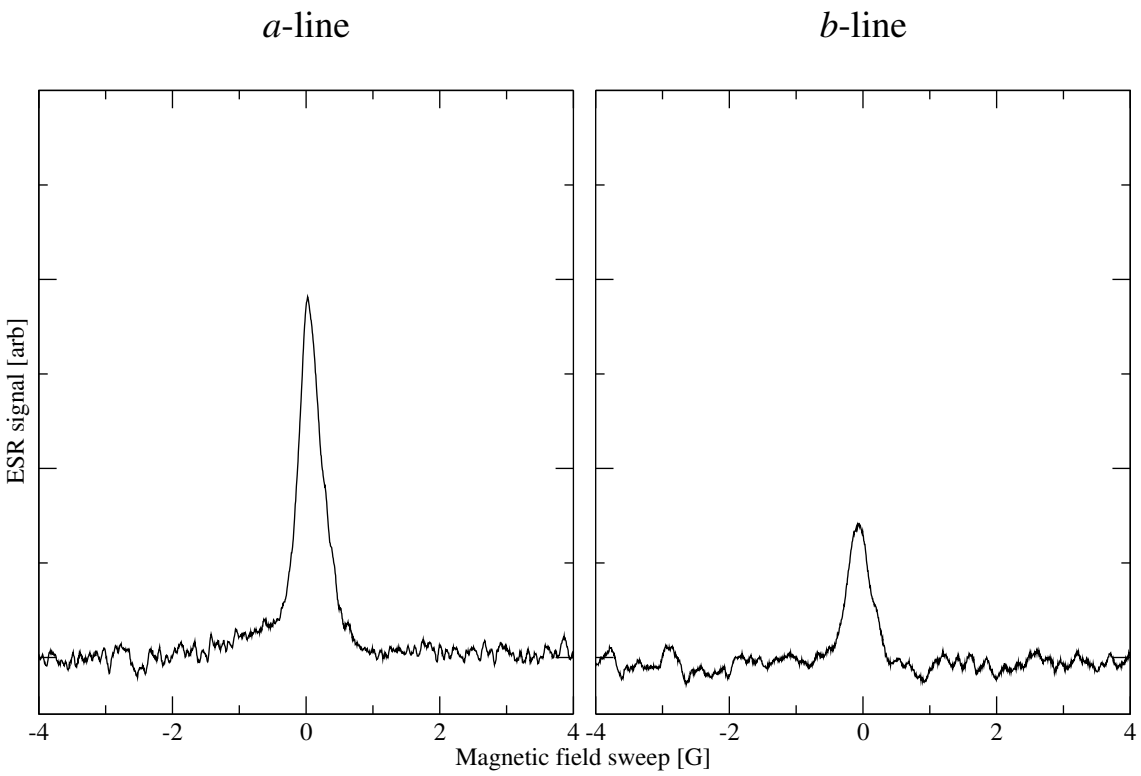

Figure 20: a- and b−line spectra after pumping H_M $a-b$ transition for ~ 5 min. H_M b-line has appeared and a-line amplitude has decreased.

b-state. Then the sweep field was stopped near $b-c$ line and RF power was applied at the calculated frequency $f_{ab\,H_M}$ with FM modulation of 50 kHz span. NMR power was set to maximum possible value which didn't yet create any heating to the SC. After 2–3 minutes of pumping, $b-c$ spectrum was recorded to detect the effect of the pumping. If no change was detected, NMR frequency was set to 50 kHz higher value and the pumping was repeated.

Scanning the frequency with such 50 kHz steps we found that some b-state population started appearing at center frequency of 908.6 MHz. Repeating the measurement and decreasing the span of the modulation we found that the transition frequency is

$$f_{ab\,H_M} = 908.63 \pm 0.03\,\text{MHz}.$$

Spectra of the largest obtained b-state population and corresponding a-state population are presented in figure 20.

Even pumping for 30 min we couldn't reach equal populations on a- and b-states. This might be due existence of several positions of H atoms in H_2 crystal splitting the resonance line to several components. Another possibility is that the field of the NMR resonator was not strong enough to saturate transition on both surfaces where H_M is detected by ESR.

Based on the experimental data we can calculate the change of hyperfine interaction constant. From equation (28) we get

$$\frac{\Delta a}{h} = 2\Delta f_{ab}. \tag{31}$$

The measured NMR frequency change is $\Delta f_{ab} = -0.66 \pm 0.03\,\mathrm{MHz}$. Measured value for the hyperfine interaction constant change is

$$\frac{\Delta a}{h} = -1.3 \pm 0.06\,\mathrm{MHz}.$$

Even with such simple experiment utilizing NMR, we get much more accurate value for Δa than with ESR. Main error in the experiment is due to large NMR frequency modulation, which was needed due to too low signal to noise ratio of the H_M ESR lines. From the measurement we also concluded that the width of the NMR transition is less than 50 kHz. Such narrow line indicates that we are dealing with good, regular crystal.

5 Conclusions

This work demonstrates possibilities of the magnetic resonance methods ESR and NMR in their application to the studies of atomic hydrogen gas. In thermal compression experiments with these methods we can directly measure both bulk and surface densities simultaneously. In addition, the methods give us information on the spatial profile of the mm-wave excitation field and on the surface density profile.

We implemented thermal detection of NMR $a - b$ transition in the bulk H$\downarrow$ gas, which cannot be done by conventional methods at so low densities. From the CW NMR spectra we extracted information on the magnetic field inhomogeneity in the NMR resonator. Implementing more sensitive recombination heat detector (e.g. bolometer), NMR studies could be used in independent measurement of the surface line shift from the bulk ESR line. Both surface line dipolar shift and wall shift could be resolved in such measurement.

For the first time we performed ESR and NMR studies of H gas inside H_2 at $T \lesssim 100\,\mathrm{mK}$. The ESR lines of H_M sample were observed simultaneously with that of the free atoms in the H$\downarrow$ gas, which allowed a first direct measurement and identification of the H_M line shifts. This reduction can be caused by an interaction of the H_M electron with the neighboring molecules. It turned out that both ESR lines of the H_M sample are shifted by $\approx 0.28 \pm 0.05\,\mathrm{G}$ towards the center of the spectrum, which implies a reduction of the hyperfine constant a, compared to that of the free atoms.

More accurate measurement of the hyperfine constant change was performed by NMR method. We succeeded in pumping the H_M $a - b$ transition and detected subsequent population change of a- and b-states from the ESR spectrum. From this experiment we obtained more accurate estimate for the hyperfine interaction constant change:

$$\frac{\Delta a}{h} = -1.3 \pm 0.06\,\mathrm{MHz}.$$

From the pumping experiments we found that the width of the H_M transition is

rather narrow, $\sim 50\,\mathrm{kHz}$. Such narrow line indicates that we are dealing with good, regular crystal.

Future improvement in the application of the ESR and NMR combination to the studies of H_M would be the increase of H_M sample size to get stronger signals. Then electron-nuclear double resonance measurements could be used to resolve more accurately the hyperfine structure of H_M.

References

[1] I. F. Silvera and J. T. M. Walraven, Spin-Polarized Atomic Hydrogen, in Progress in Low Temperature Physics, vol. X, ed. D. F. Brewer, North-Holland, Amsterdam, 1986, p. 139-370.

[2] J. T. M. Walraven, Atomic Hydrogen and Liquid Helium Surfaces, in Fundamental Systems in Quantum Optics, Les Houches Summer School LIII, 1990, ed. J. Dalibard, J. M. Raimond and J. Zinn-Justin, Elsevier Science, Amsterdam, 1992.

[3] A. I. Safonov, S. A. Vasilyev, I. S. Yasnikov, I. I. Lukashevich, and S. Jaakkola, Observation of Quasicondensate in Two-Dimensional Atomic Hydrogen, Phys. Rev. Lett. **81**, 4545 (1998).

[4] D. G. Fried, T. C. Killian, L. Willmann, D. Landhuis, S. C. Moss, D. Kleppner, and T. J. Greytak, Bose-Einstein Condensation of Atomic Hydrogen, Phys. Rev. Lett. **81**, 3811 (1998).

[5] S. Vasilyev and S. Jaakkola, Compression Experiments with 2D Atomic Hydrogen Gas on Liquid He, J. Phys. IV France **116**, 233 (2004).

[6] A. P. Mosk, Optical Study of Two-dimensional Atomic Hydrogen Gas, Ph.D thesis, University of Amsterdam, 1999.

[7] S. Vasilyev, J. Järvinen, A. I. Safonov, A. A. Kharitonov, I. I. Lukashevich and S. Jaakkola, Electron-Spin-Resonance Instability in Two-Dimensional Atomic Hydrogen Gas, Phys. Rev. Lett. **89**, 153002 (2002).

[8] B. R. Johnson, Nuclear Spin Waves in Spin Polarized Hydrogen, Ph.D thesis, Cornell University 1984.

[9] B. Yurke, Experiments on Spin Polarized Quantum Fluids, Ph.D thesis, Cornell University 1983.

[10] A. I. Safonov, S. A. Vasilyev, A. A. Kharitonov, S. T. Boldarev, I. I. Lukashevich, and S. Jaakkola, Adsorption and Two-Body Recombination of Atomic Hydrogen on ^{3}He-^{4}He Mixture Films, Phys. Rev. Lett. **86**, 3356–3359 (2001).

[11] S. Vasilyev, J. Järvinen, V. V. Khmelenko, and D. M. Lee, Experimental Observation of Atomic Hydrogen Stabilized in Thin Films of Molecular H_2 at Temperatures $\leq 100\,\mathrm{mK}$, Proceedings of LT 24, Orlando, Florida, August 2005; to be published in J. Low Temp. Phys.

[12] T. Kumada, M. Sakakibara, T. Nagasaka, H. Fukuta, J. Kumagai, and T. Miyazaki, Absence of Recombination of Neighboring H Atoms in Highly Purified Solid Parahydrogen: Electron Spin Resonance, Electron-Nuclear Double Resonance, and Electron Spin Echo Studies, J. Chem. Phys. **116**, 1109 (2002).

[13] E. Kim and M. H. W. Chan, Observation of Superflow in Solid Helium, Science **305**, 1941 (2004); Proceedings of LT 24, Orlando, Florida, August 2005.

[14] The NIST Reference on Constants, Units and Uncertainty, http://physics.nist.gov/cuu/, cited 15.11.2005.

[15] John E. Wertz and James R. Bolton, Electron Spin Resonance: Elementary Theory and Practical Applications, McGraw-Hill, New York, 1972.

[16] C. P. Slichter, Principles of Magnetic Resonance, 2nd ed., Springer-Verlag, New York, 1992.

[17] I. F. Silvera and J. T. M. Walraven, Stabilization of Atomic Hydrogen at Low Temperature, Phys. Rev. Lett. **44,** 164 (1980).

[18] C. P. Poole, Electron Spin Resonance: a Comprehensive Treatise on Experimental Techniques, Wiley, New York 1967.

[19] L. Pollack, S. Buchman and T. J. Greytak, Surface Studies of Spin-Polarized Atomic Hydrogen, Phys. Rev. B **45**, 2993 (1992).

[20] M. Mertig, E. Tjukanov, S. A. Vasilyev, A. Ya. Katunin and S. Jaakkola, Thermal Detection of ESR on Spin-Polarized Hydrogen: Study of Surface Recombination, J. Low Temp. Phys. **100,** 45 (1995).

[21] G. H. Van Yperen, ESR and Related Experiments in Spin-Polarized Atomic Hydrogen, Ph.D thesis, University of Amsterdam 1983.

[22] B. W. Statt, ESR on Spin-Polarized Atomic Hydrogen at Temperatures Below 0.5 K, Ph.D thesis, University of British Columbia 1984.

[23] S. A. Vasiliev, A. Ya. Katunin, E. Tjukanov, and I. I. Lukashevich, Production of a Nuclear Polarization in a Gas of Atomic Hydrogen by Means of a Microwave Pump, JETP Lett. **48**, 140 (1988).

[24] M. Morrow, R. Jochemsen, A. J. Berlinsky and W. N. Hardy, Zero-Field Hyperfine Resonance of Atomic Hydrogen for $0.18 \leqslant T \leqslant 1\,\mathrm{K}$: The Binding Energy of H on Liquid ^{4}He, Phys. Rev. Lett. **46**, 195 (1981); **47**, 455(E) (1981).

[25] M. W. Reynolds, I. Shinkoda, W. N. Hardy, A. J. Berlinsky, F. Bridges and B. W. Statt, Electron-Spin-Resonance Studies of Spin-Polarized Hydrogen on the Surface of Liquid ^{4}He, Phys. Rev. B **31**, 7503 (1985).

[26] I. Shinkoda and W. N. Hardy, ESR on Adsorbed Doubly Spin-Polarized Atomic Hydrogen, J. Low. Temp Phys. **85**, 99 (1991).

[27] J. L. Hall and R. T. Schumacher, Electron Spin Resonance of Hydrogen Atoms in CaF_2, Phys. Rev **127**, 1892 (1962).

[28] S. Vasilyev, J. Järvinen, E. Tjukanov and S. Jaakkola, Cryogenic 2 mm Wave Electron Spin Resonance Spectrometer with Application to Atomic Hydrogen Gas below 100 mK, Rev. Sci. Instr. **75,** 94–98 (2004).

[29] S. Vasilyev, J. Järvinen, A. I. Safonov and S. Jaakkola, Thermal Compression of Two-Dimensional Atomic Hydrogen Gas, Phys. Rev. A **69**, 023610 (2004).

[30] J. C. Collingwood and J. W. White, Helical Resonators for Spin Resonance Spectroscopy, J. Sci. Instr. **44**, 509 (1967).